Environment International 199 (2025) 109467

Contents lists available at ScienceDirect

Environment International

journal homepage: www.elsevier.com/locate/envint

Full length article

Traffic-related diesel pollution particles impair the lysosomal functions of human iPSC-derived microglia

Sohvi Ohtonen [a,1,*], Henna Jäntti [a], Luca Giudice [a], Ahmed Mohamed [a], Anastasia Shakirzyanova [a], Táňa Závodná [b], Ilya Belevich [c], Hong Yan [d], Angélica María Sabogal-Guáqueta [d,e], Liudmila Saveleva [a], Mari-Anna Väänänen [a], Ashley Rillo-Albert [a,2], Elisa Perciballi [a,f], Daniela Ferrari [f], Minna-Mari Tervo [a], Mireia Gómez-Budia [a], Zdeněk Krejčík [b], Päivi Aakko-Saksa [g], Jari Koistinaho [a,3], Šárka Lehtonen [a], Katja M. Kanninen [a], Jan Topinka [b], Eija Jokitalo [c], Alejandra Sierra [a], Martina Schmidt [d,h], Amalia M. Dolga [d,h], Pasi I. Jalava [i], Paula Korhonen [a,†], Tarja Malm [a,†,*]

[a] A.I. Virtanen Institute for Molecular Sciences, University of Eastern Finland, Kuopio, Finland
[b] Department of Toxicology and Molecular Epidemiology, Institute of Experimental Medicine of the Czech Academy of Sciences, Prague, Czech Republic
[c] Electron Microscopy Unit, Institute of Biotechnology, Helsinki Institute of Life Science, University of Helsinki, Helsinki, Finland
[d] Department of Molecular Pharmacology, Groningen Research Institute of Pharmacy, Faculty of Science and Engineering, University of Groningen, the Netherlands
[e] Department of Molecular Cell Biology and Immunology, Amsterdam UMC, Vrije Universiteit Amsterdam, Amsterdam, the Netherlands
[f] Department of Biotechnology and Bioscience, University of Milano-Bicocca, Milan, Italy
[g] VTT Technical Research Centre of Finland, Espoo, Finland
[h] Groningen Research Institute for Asthma and COPD (GRIAC), University of Groningen, University Medical Center Groningen, Groningen, the Netherlands
[i] Department of Environmental and Biological Science, University of Eastern Finland, Kuopio, Finland

ARTICLE INFO

Editor: Dr Frederic Coulon

Keywords:
Human microglia
iPSC
Air pollution
Lysosome
Diesel

ABSTRACT

Exposure to air pollution is associated with neurological diseases. Traffic is a major source of air pollution, consisting of a complex mixture of ultrafine particles, that can invade the brain and induce a microglia-mediated inflammatory response. However, the exact mechanisms of how traffic-related particles impact human microglia remain poorly understood.

This study investigates the effects of diesel exhaust particles (DEPs) on human induced pluripotent stem cell-derived microglia-like cells (iMGL). We exposed iMGLs to three different DEPs and studied the impact on the iMGL transcriptome and functionality, focusing on cytokine secretion, mitochondrial respiration, lysosomal function, and phagocytosis. A20 particles were collected from a heavy-duty engine run with petroleum diesel. For A0, the same engine was run with renewable diesel. E6 was produced with a modern 2019 model diesel passenger car run with renewable diesel. RNAseq revealed activation of the cytokine storm pathway and inhibition of the autophagy pathway in iMGLs after exposure to particles derived from older diesel emission technology (A20, A0). Particles from the modern diesel engine technology (E6) did not alter microglial transcriptome after 24 h exposure. A20 and A0 exposure led to impaired lysosomal functions in iMGLs. In contrast, E6 did not cause major alterations in microglia functions. In addition, we show that response to particles is more pronounced in human iMGLs compared to mouse primary microglia.

To conclude, particles from older emission technology impair phago-lysosomal functions of iMGLs, but modern alternatives with filtration do not induce drastic changes in the functionality of iMGLs.

* Corresponding authors.
E-mail addresses: sohvi.ohtonen@uef.fi (S. Ohtonen), tarja.malm@uef.fi (T. Malm).
[1] Present address: Department of Physiology and Pharmacology, Karolinska Institute, Solna, Stockholm, Sweden.
[2] Present address: CÚRAM, SFI Research Centre for Medical Devices, University of Galway, Galway H92 W2TY, Ireland.
[3] Present address: Helsinki Institute of Life Science, and Drug Research Program, Division of Pharmacology and Pharmacotherapy, University of Helsinki, Helsinki, Finland.
[†] These authors have equal contribution.

https://doi.org/10.1016/j.envint.2025.109467
Received 20 December 2024; Received in revised form 14 March 2025; Accepted 13 April 2025
Available online 5 May 2025

1. Introduction

Exposure to air pollution has been linked with a variety of adverse health effects in the lungs and heart, and recently, it has also been associated with cognitive decline and neurodegeneration (Cristaldi et al., 2022; European Environment Agency, 2023). The European Environment Agency estimated that in 2021, 97 % of the urban population was exposed to levels of pollution exceeding the newest World Health Organization guidelines (European Environment Agency, 2023; World Health Organization, 2021). A major source of outdoor pollution is traffic-related air pollution, consisting of a complex mixture of gaseous and particulate compounds, such as diesel exhaust particles (DEPs) (Wichmann, 2007). The size of the DEPs can reach the nanometer range and are classified as ultrafine particles (UFPs) with an aerodynamic diameter of less than 100 nm (Liati et al., 2018). Even though the levels of particulate matter are regulated, no legal ambient standards for UFPs exist. However, WHO recommends increasing the research knowledge of UFPs (World Health Organization, 2021).

The smaller particles are the most concerning, and inhaled particles can quickly penetrate different tissues (Kwon et al., 2020). A variety of nanoparticles have been detected in human lungs and serum (Lu et al., 2020). Growing evidence shows that particles can also be deposited in the brain. Isotope-labeled carbon black molecules have been reported to be distributed rapidly to the brain among other organs (Qi et al., 2022), and different nanoparticles and black carbon particles have been found in the human brain (Maher et al., 2016; Vanbrabant et al., 2024). Strikingly, black carbon from maternal exposure has also been reported to be present in the placenta and even in fetal organs, including the developing brain (Bongaerts et al., 2022; Bové et al., 2019). Exposure to diesel exhaust can lead to alterations in memory and behaviour in mice (Ehsanifar et al., 2023, 2022, 2021; Li et al., 2020). Even a short exposure to diesel particles can lead to increased cytokine levels and oxidative stress in mouse brain (Cole et al., 2016; Shkirkova et al., 2022). Cortical stress response and decreased brain connectivity in humans have been reported as well (Crüts et al., 2008; Gawryluk et al., 2023).

The specialized immune cells of the brain, microglia, are the first to respond to brain-infiltrating particles. Upon current knowledge, microglial dysfunction is also considered as the potential initiator of inflammatory events in the central nervous system associated with neurodegenerative diseases such as Alzheimer's disease or Parkinson's disease (Zhang et al., 2023). Exposure to air pollution has been raised as a potential contributor to microglial dysfunction and has been extensively studied in rodent microglia. However, recent research has demonstrated that human and rodent microglia differ from each other in their transcriptome and functions (Abels et al., 2021; Galatro et al., 2017; Sabogal-Guáqueta et al., 2023; Yvanka de Soysa et al., 2022). Yet, we still have limited knowledge of how pollution impacts human microglia.

Stem cell-derived human microglia recapitulate the important transcriptomics signatures and functions of human microglia and offer a simple but more translationally relevant tool to study air pollutant exposure in human microglia (Dolan et al., 2023; Hedegaard et al., 2020; Lloyd et al., 2024; Speicher et al., 2019). Here we elucidated how three different diesel exhaust −derived particles impact the human induced pluripotent stem cell (iPSC)-derived microglia-like cells (iMGLs). We have previously published a smaller-scale study, describing that particulate matter originating from a diesel car engine or a bus run with compressed natural gas can alter human microglial functions (Jäntti et al., 2024). To broaden these findings on diesel exhaust, we utilized emissions derived from a heavy-duty diesel engine run either with petroleum diesel with a fuel aromatic content of 20 % (A20) or renewable diesel with 0 % aromatic content (A0), or from a 2019 model diesel car run with renewable diesel (E6). We chose a concentration of DEPs that did not alter the viability of the cells to study how short-term exposure alters the microglial transcriptome. To validate the transcriptomic findings, we carried out a specific panel of functional assays to investigate the effect of the particles on microglial cytokine secretion, mitochondrial respiration, phagocytosis and lysosomal function. We hypothesized that short-term exposure to DEPs can elicit a strong inflammatory response in iMGLs due to a complex mixture of components. Our results indicate that exposure to DEPs disturbs the microglial transcriptome and function depending on the engine, fuel, and emission aftertreatment technology. Thus, this study contributes to understanding the impact of traffic-related air pollution, specifically diesel exhaust, on human brain health.

2. Results

2.1. Diesel exhaust particles are not toxic to iMGLs in any tested concentrations

To study the impact of DEPs on human microglia, iPSCs derived from clinically healthy individuals were differentiated into iMGLs (Konttinen et al., 2019) and exposed to particles (A20, A0, or E6). A20 and A0 are derived from a modern heavy-duty diesel engine without any aftertreatment system, thus presenting diesel exhaust from older emission technology. A20 was produced with standard EN590 petroleum diesel and A0 with renewable EN15940 diesel. For E6, a 2019 diesel vehicle was run with renewable diesel, and it presents the most modern diesel exhaust compliant with the Euro 6d European emission standard. These particles have been characterized previously (Hakkarainen et al., 2023; Mussalo et al., 2023). The size of the particles was less than 100 nm in diameter and thus, they are defined as ultrafine particles. To expose iMGLs, the exhaust particles were extracted from collection filters to a solvent containing DMSO, diluted directly into the medium, and introduced to the cells (Fig. 1A). For the comparison of particle effect, either solvent control or a filter control was used. For solvent control, the same concentration of DMSO was used as in particle exposure. For the filter controls (FC-A for A20 and A0; FC-E for E6), clean filters were processed similarly to particle collection filters but without exposure to the diesel exhaust.

First, the potential cytotoxicity of the particles was assessed with live-cell imaging. iMGLs were exposed to several concentrations of particles or a corresponding concentration of solvent control (DMSO) for 24 h. After the addition of the DMSO control or pollutants, a small peak in cytotoxicity signal was observed within the first hours from starting the exposure (Supp. Fig. S1A-B). This was also evident in the untreated medium control (without any exposure) and it vanished within a couple of hours. After 24 h, none of the tested concentrations were cytotoxic for iMGLs. Additionally, the impact of the exposure on the metabolic activity of iMGLs was measured by MTT assay. Increasing concentrations of A20 and A0 caused an increasing trend in metabolic activity, and the highest concentrations of A20 and A0 caused a statistically significant increase in the metabolic activity compared to DMSO control (Supp. Fig. S2A). In iMGLs exposed to E6, there were no changes in the metabolic activity compared to the DMSO control in any of tested concentrations.

Even though these pollutants have been described as ultrafine particles (Mussalo et al., 2023), A0 and A20 had some particle agglomerates visible on normal light microscope in a dose-dependent manner (Supp. Fig. S2B). However, as these A20 and A0 contain a combination of carbon particles (Hakkarainen et al., 2023), they are susceptible to forming aggregates in solutions. The particle number in E6 is extremely low compared to A20 and A0, no visible aggregates were seen at any concentration.

The concentration of particle exposure was equalized to the following assays and set to 50 L of collected exhaust/mL (with 0.25 % DMSO). As a mass, this corresponds to 132.5 μg/mL for A20 and 90 μg/mL for A0. As E6 presents the most modern technology, it produced only negligible mass and thus, cannot be reported as such. These can be considered as a high dose, as earlier studies have used pollutant

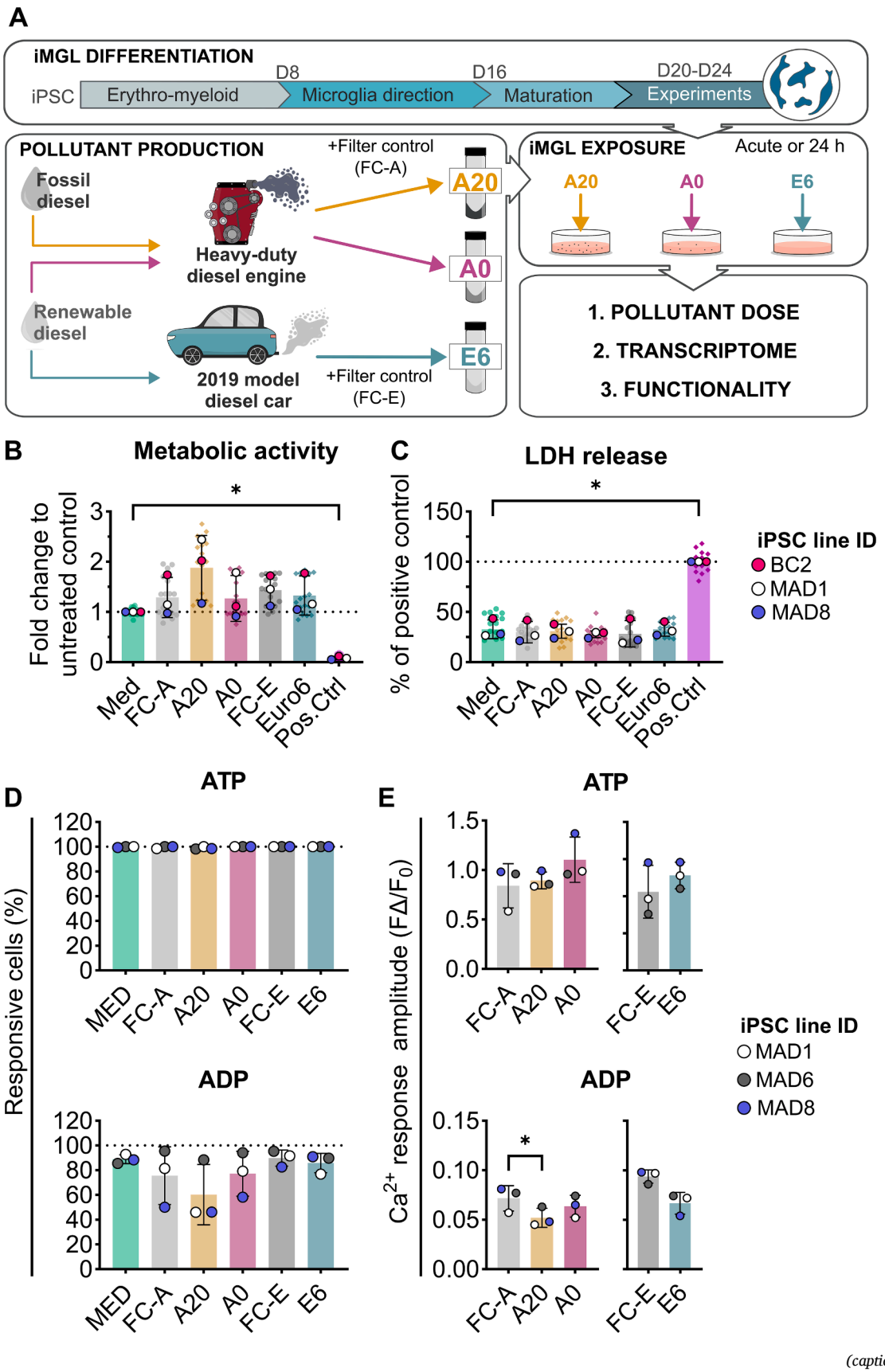

(caption on next page)

Fig. 1. Exposure and cytotoxicity of three diesel-exhaust derived pollutants in iMGLs A) workflow of the study. Pollutants from diesel exhaust were collected in filters and extracted. Particles were dissolved and introduced to cells in the culture medium. The iMGLs were exposed to pollutants for 24 h and the cytotoxicity was evaluated by measuring B) the metabolic activity with MTT-assay and C) LDH release. n = 3 (iPSC lines, outlined symbols), each with 4–6 technical replicates (wells, non-lined symbols). Comparison to corresponding filter control (FC-A vs. A20 or A0, FC-E vs. E6) with matched one-way ANOVA with Šidák multiple comparisons test. D) Percentage of cells with intracellular Ca^{2+} response to acute application of 100 μM ATP or ADP after 24 h exposure to pollutants. E) Amplitude of ATP- or ADP-induced intracellular Ca^{2+} transient. n = 3 (iPSC lines), with the number of cells recorded per group 89–322 and the median used to describe the population. The data is presented as mean ± SD. Matched one-way ANOVA with Dunnett's multiple comparison test (FC-A vs. A20 or A0) or paired *t*-test (FC-E vs. E6) was used, p-value=*<0.05. iPSC = human induced pluripotent stem cells, iMGLs = human induced microglia-like cells. Diesel exhaust pollutants: A20 = heavy-duty engine run with petroleum diesel, A0 = heavy-duty engine run with renewable diesel, E6 = a 2019 model diesel vehicle run with renewable diesel, FC-A = filter control for A20 and A0 pollutants, FC-E = filter control for E6. Med = untreated medium control.

concentrations varying from 1 to 100 μg/mL for 24 h exposure, mostly for mouse microglial cell line (BV2) or primary mouse microglia (Gómez-Budia et al., 2020; Jäntti et al., 2024; Kang et al., 2021). We confirmed that these concentrations did not significantly alter the metabolic activity or release of lactate dehydrogenase (LDH) of iMGLs (Fig. 1B–C). In addition, after 24 h exposure to particles, iMGLs responded to acute application of ATP and APD and showed an increase in intracellular Ca^{2+} (Fig. 1D). iMGLs responded to ATP equally in all exposure groups (>98 % of cells responsive). The percentage of cells responding to ADP showed a decreasing trend in A20-exposed iMGLs, but the difference was not significant. The amplitude of ADP-induced Ca^{2+} signal was significantly decreased in iMGLs after exposure to A20 (Fig. 1E). No other significant differences in signal amplitude were observed. Finally, immunostaining showed that iMGLs expressed markers of microglial identity, including IBA1, PU.1, P2RY12, and TMEM119 after 24 h exposure (Supp. Fig. S3).

2.2. Exposure to A0 and A20 alter pathways associated with microglial functions

To investigate whether cellular processes are altered due to particle exposure, we analyzed the transcriptome of iMGLs after 24 h of exposure (Fig. 2A). As a comparison, lipopolysaccharide (LPS) was used as a positive control to induce a strong inflammatory stimulus for iMGLs. RNA sequencing revealed 1994 and 399 differentially expressed genes (DEGs) in A20- and A0-exposed iMGLs, respectively (Fig. 2B). 355 DEGs were common between A20- and A0-exposed iMGLs. Unexpectedly, E6 exposure did not reveal any DEGs. LPS stimulation induced a stronger response in the iMGLs transcriptome, with around 5800 DEGs (Supp. Fig. S4A, Supp. Tables S1 and S2). Whilst some of the DEGs were shared between A20 or A0 exposure, LPS induced a distinct transcriptional response compared to the particle exposures (Supp. Fig. S4A). iMGLs retained their transcriptional microglial identity upon exposure (Supp. Fig. S4B).

The most upregulated genes in response to A20 and A0 exposure included e.g. *IL8, IL1B, TNF, CLEC5A, THBP,* and *NQ1A* (Supp. Table S1). Functional enrichment analysis of DEGs found several deregulated pathways, which were shared between A20- and A0-exposed iMGLs (Fig. 2C, Supp. Table S3.). As expected, pathways associated with particle exposure such as "xenobiotic metabolism" and "aryl hydrocarbon receptor signaling" had positive z-scores and were predicted to be activated. In addition, pathways related to the cell cycle were predicted to be activated. In addition, activation of either ferroptosis (A20) or pyroptosis (A0) signaling pathways suggests cellular stress in response to the particles.

The analysis also revealed alterations in pathways associated with multiple important microglial functions, such as the upregulation of cytokine and chemokine genes translated as activation of the "hypercytokinemia/hyperchemokinemia pathway". In addition, phagocytosis and autophagy pathways were inhibited, possibly disturbing the clearance capacity of iMGLs. Finally, activation of pattern recognition receptors and TREM1 signaling was predicted. The analysis also revealed some unique pathways associated with A20 exposure (Supp. Fig. S4C, Supp. Table S3). These included, for example, activation of cholesterol biosynthesis, CLEAR (Coordinated Lysosomal Expression and Regulation) signaling, and production of nitrite oxide and reactive oxygen species pathways.

2.3. Transcriptional signature specific for human microglia

To investigate whether the transcriptional changes detected in the particle-exposed iMGLs are specific to human microglia, we exposed mouse primary microglia to A20 or A0 in a similar manner (Fig. 2D). Due to the limited amount of filter control, we utilized 0.25 % DMSO as a control. Analysis revealed 2670 DEGs in A20-exposed and 9 DEGs in A0-exposed mouse microglia in comparison to DMSO control (Supp. Table S4). Compared to iMGLs, the induced transcriptional changes were lower in magnitude, especially in A0-exposed mouse microglia. In iMGLs, 3150 DEGs and 645 DEGs were observed in A20- and A0-exposed iMGLs when compared to DMSO control, respectively (Supp. Table S1).

Pathway enrichment analysis was carried out to evaluate if the exposure alters similar pathways in both human iMGLs and mouse microglia. In A20-exposed microglia, most of the pathways were shared between human iMGLs and mouse microglia (Fig. 2E). These pathways were related to cell cycle regulation and immune response and, for example, included alterations in TREM1 signaling, cytokine storm, autophagy, and phagocytosis pathways (Supp. Table S5). In contrast, exposure to A0 caused mostly changes in the human iMGLs. For example, the analysis did not predict alterations in autophagy, phagocytosis, and immune-related pathways in A0-exposed mouse microglia in contrast to human iMGLs (Supp. Table S5). In mouse microglia, the alterations were mostly related to amino acid metabolism. Only six pathways were shared between A0-exposed iMGLs and mouse microglia. These shared pathways included: "Cristae formation", "Regulation of lipid metabolism by PPARalpha", and "Transport of inorganic cations/anions and amino acids/oligopeptides". In addition, three pathways ("Mitochondrial protein import", "Xenobiotic Metabolism AHR Signaling Pathway", and "tRNA Charging") were also shared among all the groups.

2.4. Exposure to A20 and A0 increase the gene transcription of cytokines and chemokines, but this is not replicated at the protein level

As exposure to A20 and A0 increased the gene transcription of several cytokines and chemokines (e.g. *IL8, IL10, IL1B, CCL3)* (Fig. 3A), we measured the cytokine and chemokine secretion from iMGLs after 24 h exposure to particles. The levels of IL-1β were detectable in the medium samples of iMGLs only from one iPSC-line (MAD6), and the levels of TNFα were under the detection limit in iMGLs from one iPSC-line (MAD8). The secretion of IL-10 was significantly lower in A20- and A0-exposed iMGLs compared to the filter control (Fig. 3B). In addition, the levels of MIP1α/CCL3, IL-8, and IL-6 showed a trend towards lower secretion in A20-exposed iMGLs, however, the difference failed to reach statistical significance. E6 exposure did not cause any significant differences in any of the measured analytes.

2.5. Exposure to A20 and E6 cause minor alterations in the mitochondrial respiration of iMGLs

To investigate if particle exposure causes changes in the metabolism

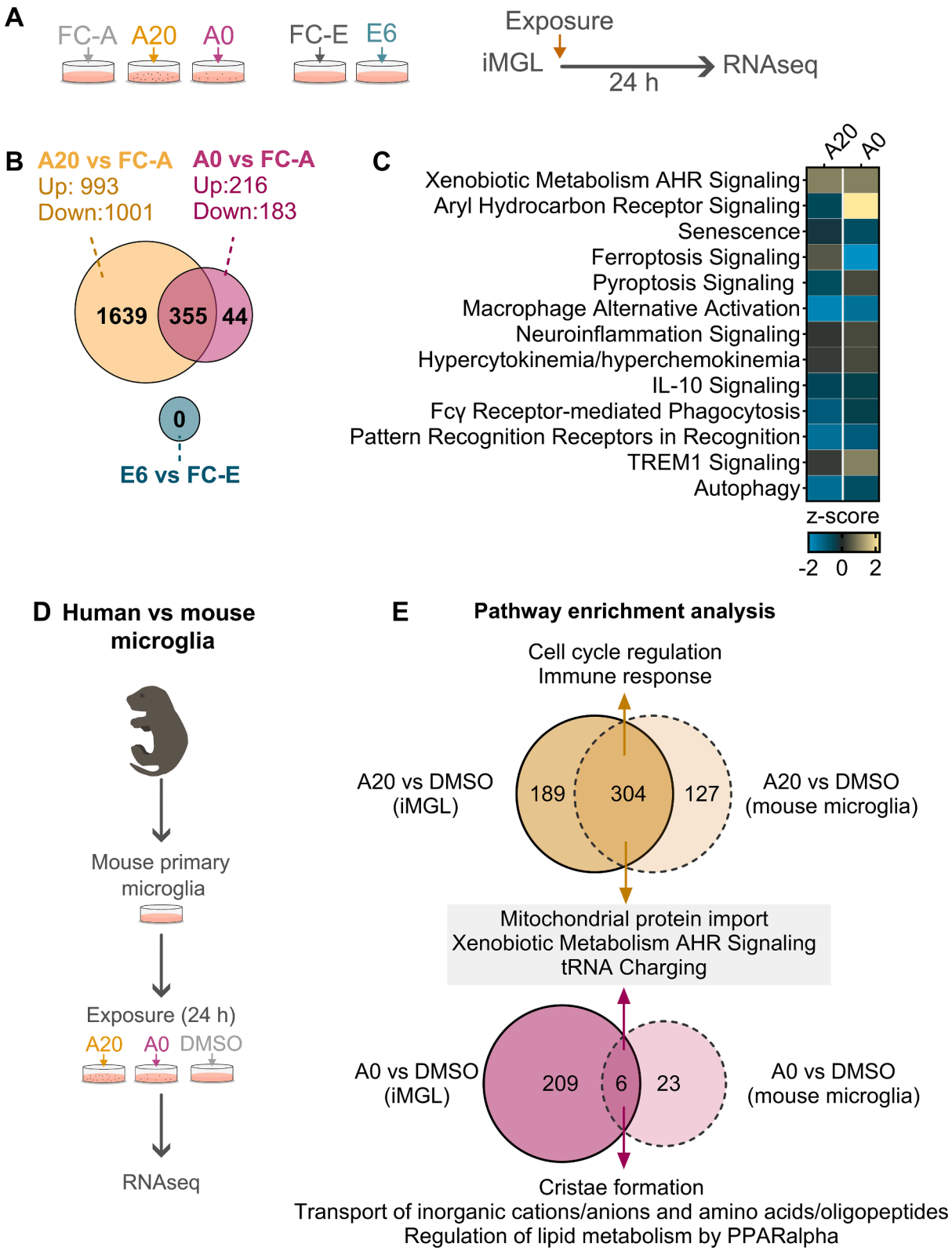

Fig. 2. Impact of pollutant exposure on the transcriptome of iMGLs. A) iMGLs were exposed to pollutants for 24 h and changes in iMGLs transcriptome were studied. B) Number of differentially expressed genes (DEGs) between pollutant treatment and corresponding filter control exposure. C) Pathway analysis of DEGs with heatmap presentation of shared pathways between A20 and A0 exposure. Yellow indicates activation in exposed samples; blue indicates inhibition in exposed samples, n = 8 for A20, A0, and FC-A, n = 7 for E6, and n = 4 for FC-E (iPSC lines) with one technical replicate (dish) per each sample. D) To compare human-specific transcriptional changes, primary microglia were extracted from mouse pups and exposed to A20 and A0 pollutants. DMSO was used as a control. E) Pathway enrichment analysis revealed shared and unique pathways in human iMGLs and mouse microglia upon A20 or A0 exposure. For mouse microglia, n = 7 (DMSO), 5 (A0) and 6 (A20) of primary microglia culture batches. For iMGLs, n = 8 iPSC lines (A20, A0, DMSO). (For interpretation of the references to color in this figure legend, the reader is referred to the web version of this article.)

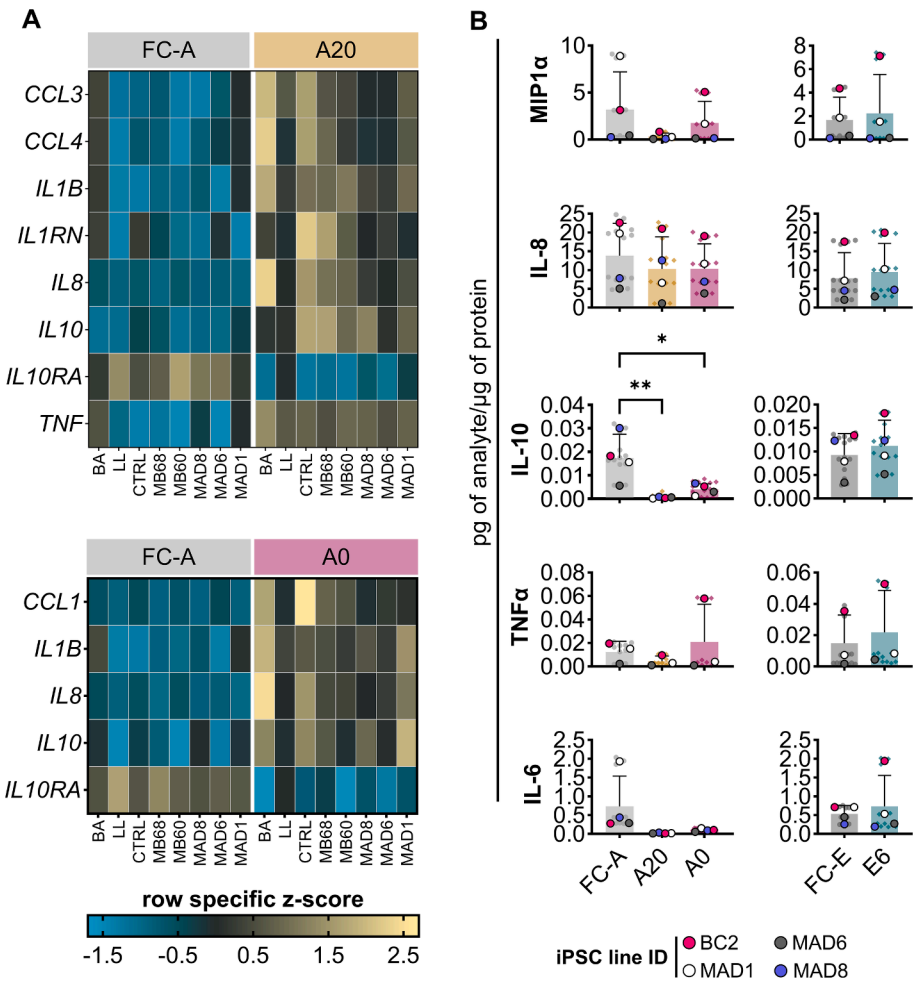

Fig. 3. Impact of air pollutant iMGLs cytokine expression and secretion. A) Differentially expressed cytokine and chemokine genes in A20 and A0 exposed iMGLs, presented as z-score for each row (n = 8 iPSC lines, in columns). B) MIP1α/CCL3, IL-8, IL-10, TNFα, and IL-6 measured from the medium after 24 h exposure. n = 3–4 (lines, symbols with black outline) with 3–4 technical replicates (wells, non-lined symbols). The data is presented as mean ± SD. Matched one-way ANOVA with Dunnetts multiple comparison test (FC-A vs. A20 or A0), or paired *t*-test used (FC-E vs. E6), p-value = *<0.05, ** <0.01.

of iMGLs, we employed Seahorse Mito Stress assay after 24 h exposure. The assay measures cellular oxygen consumption rate (OCR) in response to the injection of chemicals modulating mitochondrial functions (Fig. 4A, D), which enables the estimation of parameters reflecting cellular respiration. Exposure to A20 led to a significant increase in the proton leak of iMGLs, but A0 or E6 exposure did not result in any significant changes in these parameters (Fig. 4B, E). The basal extracellular acidification rate (ECAR) was significantly decreased after E6 exposure in iMGLs, but no ECAR changes were observed in A20- or A0-exposed iMGLs (Fig. 4C, F).

2.6. Exposure to E6 leads to enhanced motility of iMGLs

After exposure to particles, iMGLs showed a normal response to ADP application with increase in intracellular Ca^{2+} (Fig. 1D–E). ADP is also a strong chemotaxis-inducing agent and thus, we investigated if particle exposure can alter the motility of iMGLs. We utilized scratch wound assay and measured the migration of iMGLs on the wound area (relative wound density, RWD) upon acute exposure. In A20, the particles accumulated in the wound area (Supp. Fig. s5A). As the assay relies only on the phase image, the quantification of A20 exposure on the cellular motility was not feasible. However, no quantification bias was observed in A0- or E6-exposed iMGLs (Supp. Fig. S5B). ADP induced faster migration to the wounded area (Supp. Fig. S5C). No significant differences were observed in the basal motility upon A0 exposure; however, E6 increased the motility of iMGLs (Supp. Fig. S5D). No differences were observed in ADP-induced motility in response to either of the pollutants.

2.7. Exposure to A20 and A0 alter the lysosomal dynamics of iMGLs

As analysis of RNAseq data predicted alterations in the lysosome-phagocytic pathway of microglia, we examined the impact of exposure on iMGLs lysosome function (Fig. 5A). As a proxy estimation for lysosomal functions, iMGLs were stained with a lysosomal dye (Lysoview 540) which incorporates the acidic lysosome and exhibits fluorescence in an acidic environment. With live-cell imaging of the iMGLs, we detected a striking reduction in lysosomal staining after acute exposure to A20 or A0 (Fig. 5B, Supp. Fig. S6A) and quantification showed a significant decrease in the Lysoview 540 intensity already at two hours after starting the exposure (Fig. 5B). E6 did not cause any alterations in the lysosomal function.

As the RNAseq analysis of mouse primary microglia suggested that A20, but not A0, induces alterations in the pathways involved in the lysosomal system, we repeated the Lysoview assay also using mouse microglia. We detected a significant reduction in the Lysoview 540 intensity in A20- or A0-exposed mouse microglia (Supp. Fig. S7A-B). However, compared to iMGLs, the reduction was slower and less drastic (Supp. Fig. S7C-D). In iMGLs, two hours after starting the exposure, the Lysoview540 intensity was less than 15 % from the zero timepoint (T0 = 100 %) in A20- and A0-exposed iMGLs. Whilst, in the control, the value

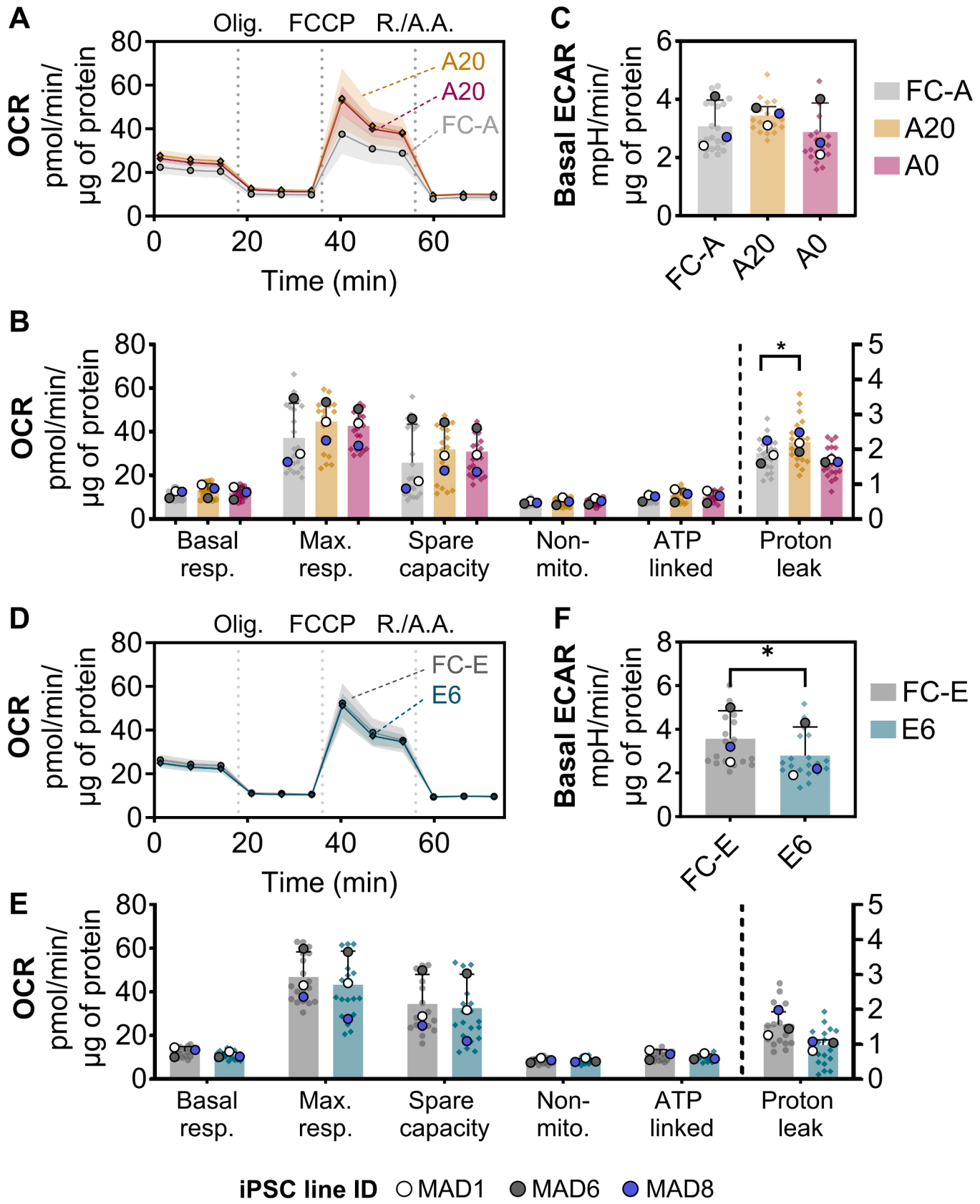

Fig. 4. Impact of air pollutant exposure on iMGLs mitochondrial respiration. The mitochondrial respiration of iMGLs after 24 h exposure was measured with Mito Stress assay. A and D) representative oxygen consumption rates (OCR) for each exposure, n = 1 line with 6–8 technical replicates (wells). B and E) mitochondrial parameters calculated from OCR. C and F) basal extracellular acidification rate (ECAR). n = 3 (iPSC lines, outlined symbols) calculated as average from 3 to 8 technical replicates (wells, non-lined symbols). The data is presented as mean ± SD. Matched two-way ANOVA with Šidák multiple comparison test (B, E), paired one-way ANOVA with Dunnetťs multiple comparison test (C) or paired *t*-test (F), p-value= *<0.05.

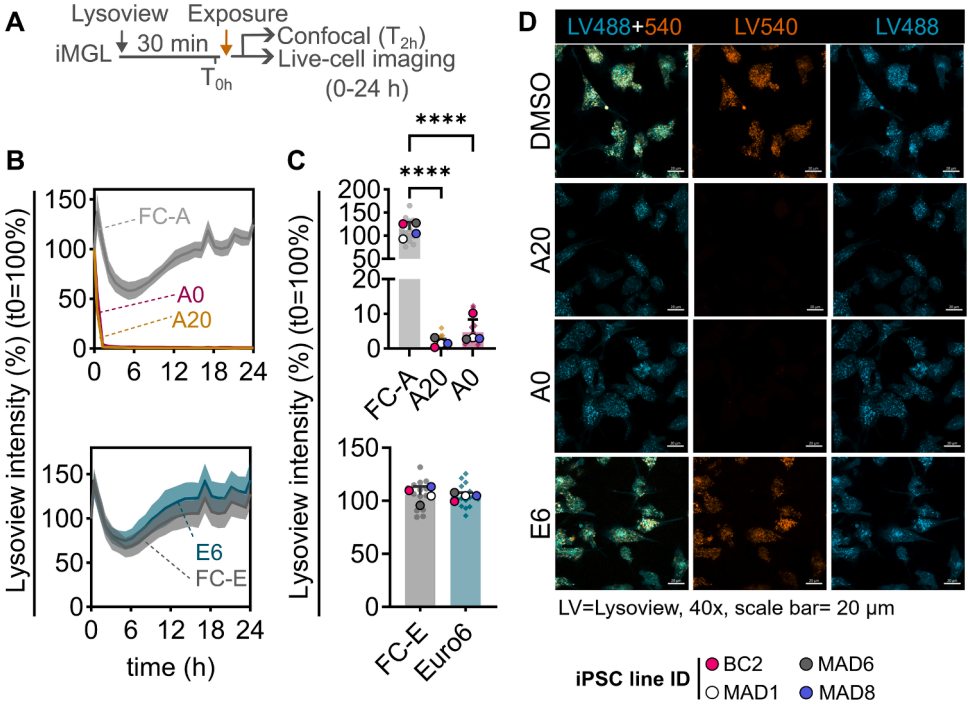

Fig. 5. Impact of pollutant exposure on iMGLs lysosomal function. The dynamics of lysosomal staining were measured with live-cell imaging upon acute exposure to pollutants. A) Workflow of the lysosomal assay. B) Representative curves of Lysoview fluorescence intensity upon time, n = 1 iPSC line, with 3–5 technical replicates (wells). C) Quantified lysosome fluorescence intensity at 2 h after starting the exposure, data normalized to first timepoint (T_0 = 100 %). The data is presented as mean ± SD. n = 4 (iPSC lines, outlined symbols) with 3–5 technical replicates (wells, non-lined symbols). Paired two-way ANOVA with Dunnett's multiple comparison test, p-value=****<0.001 D) Representative confocal microscope images when the lysosomal staining was visualized with higher resolution after 2 h exposure. Lysoview 488 (green) is presented as turquoise for better visualization. Lysoview 540 is presented as orange. The experiment was repeated with iMGLs differentiated from two iPSC lines with similar results. (For interpretation of the references to color in this figure legend, the reader is referred to the web version of this article.)

remained at 100 %. In mouse microglia, the Lysoview540 intensity increased after two hours of exposure to 130–140 % in the control, and the intensity in A0 exposure was around 100–120 %, and in A20 around 65–100 %.

As the intensity of Lysoview 540 is pH-dependent, we hypothesized that the reduction was due to changes in the lysosomal pH. To confirm this finding at a higher resolution, we utilized Lysoview 540 in combination with Lysoview 488 and confocal imaging. Lysoview 488 accumulates in acidic intracellular organelles but the fluorescence is not pH-dependent and should be retained in the lysosome even upon changes in the pH. All the particle-exposed iMGLs showed positive staining of lysosomal structures as detected using Lysoview 488 (Fig. 5C, Supp. Fig. S6C). However, as we noticed previously, the fluorescence of Lysoview 540 decreased significantly upon exposure to A20 or A0. In E6-exposed iMGLs, both lysosomal dyes were visible. In all the exposures, we noticed that the lysosomes moved inside the cells during the imaging. Thus, quantification or co-localization analysis of the lysosomal structures was unreliable using this imaging setup.

2.8. Exposure to A20 and A0 dampen the phagocytosis and alter the cellular structure of iMGLs

As lysosomal dysfunction can impair the phagocytic capacity of iMGLs, we investigated if the phagocytosis of Zymosan-labelled pHrodo bioparticles was altered. After 24 h particle exposure, iMGLs were fed with bioparticles, and phagocytosis was observed with live-cell imaging for six hours (Fig. 6A). Clearance of bioparticles in the vicinity of iMGLs was observed in all the exposures and increasing cytosolic fluorescence of internalized pHrodo particles was detected (Fig. 6B–C, Supp. Fig. S6B). However, A20- and A0-exposed iMGLs showed significantly reduced fluorescence intensity. In line with the previous results, E6 did not cause any significant alterations in the phagocytosis of iMGLs.

Finally, we explored the impact of particle exposure on the overall intracellular structure of iMGLs with serial block face scanning electron microscopy. The iMGLs exhibited heterogeneity in the cellular structure (Fig. 6D,G, Supp. Fig. S8). In the filter controls, the iMGLs had a high number of translucent vacuole structures as well as smaller, darker lysosomes and elongated mitochondria (Fig. 6D,G). However, some cells were more electron-dense, and the cytoplasm appeared darker (Fig. 6Gi). In FC-A, located near the nucleus (N), we observed a bigger, gastrosome-like structure (G) (Villani et al., 2019). In the A20- and A0-exposed iMGLs, we observed a higher number of dark lysosomes and disruption in the vacuole structure (Fig. 6E–F). We did not observe similar major alterations in E6-exposed iMGLs and detected only slightly larger vacuole structures (Fig. 6H).

3. Material and methods

3.1. Study design

In vitro, a human induced pluripotent stem cell-derived model of human microglia (iMGLs) was used to study the impact of diesel-derived pollution on human microglia. All work followed the World Medical Association Declaration of Helsinki (World Medical Association, 2013), and national guidelines. The iPSC lines used in this study originate from clinically healthy individuals from more than one source. No extensive characterization of any neurodegeneration-associated risk factors has been carried out, but all the lines were APOE ε3 carriers. For the quantification of the functional testing, at least three technical replicates were used, and the assay was carried out with iMGLs differentiated from at least three different iPSC lines. Due to the limited availability of the pollutants, it was not possible to carry out more independent

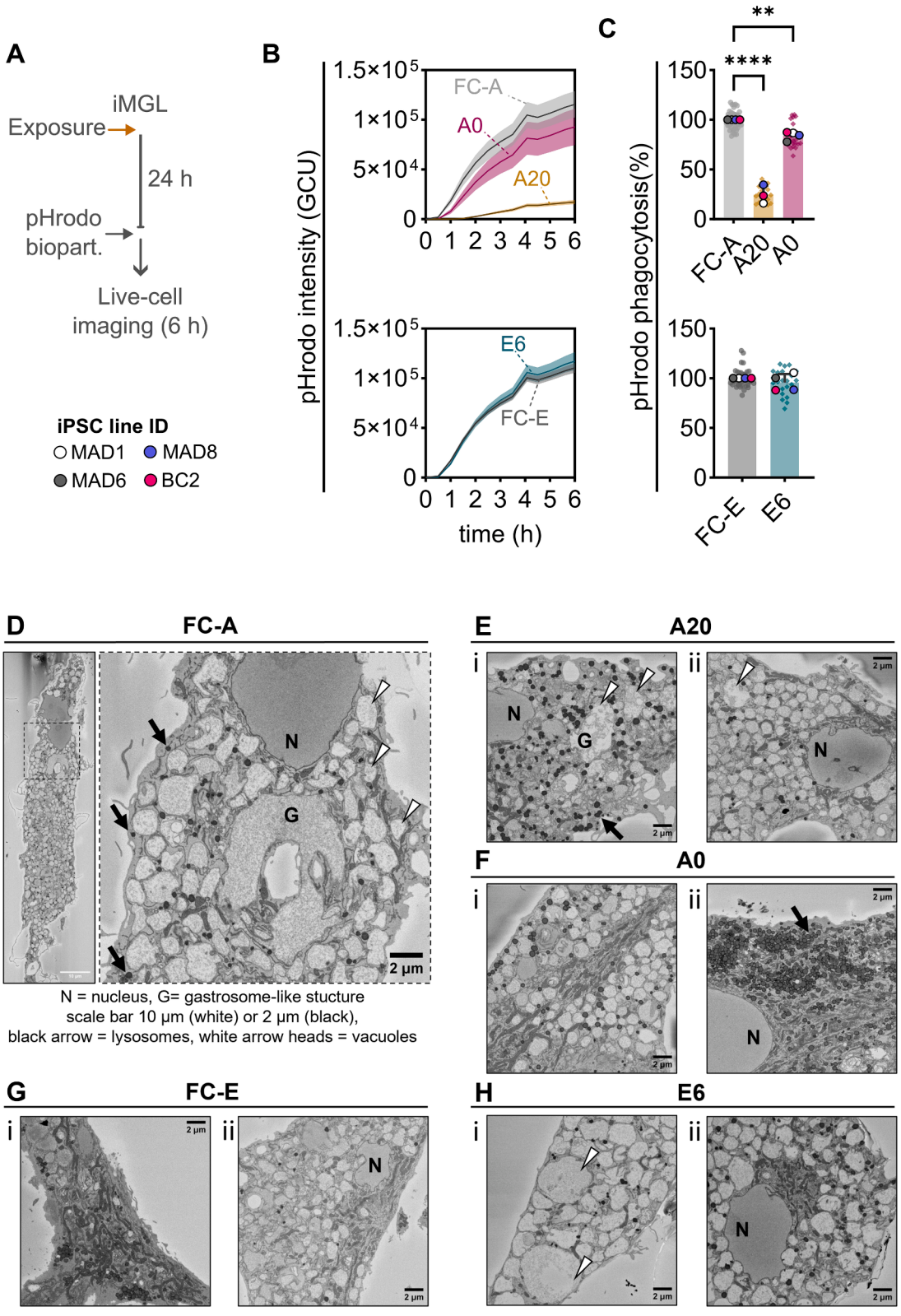

Fig. 6. Impact of pollutant exposure on iMGLs phagocytosis and cellular structure. Phagocytosis of pHrodo labeled bioparticles by iMGLs was measured after 24 h exposure to pollutants. A) Workflow of the phagocytosis assay. B) representative time curve of phagocytosis for 6 h, n = 1 biological replicate, with 5–6 technical replicates (wells). C) Quantified phagocytosis after 6 h, n = 3–4 biological replicates (iPSC lines, lined symbols), with 4–12 technical replicates (wells, non-lined symbols), normalized to the corresponding control. The data is presented as mean ± SD. Matched one-way ANOVA with Dunnetts multiple comparison test or paired *t*-test. P-value= **<0.01, ****<0.0001. The ultrastructure of iMGLs after 24 h exposure was analyzed with serial block-face scanning electron microscopy. D-H) Representative electron micrographs of exposed iMGLs. The experiment was carried out with one genotype (BC2).

replications of the assays. To evaluate the species difference between mouse and human microglia, the most prominent assays were replicated in mouse primary microglia.

The exposure of iMGLs to diesel-derived pollutants was carried out by introducing the pollutants directly into the culture medium. As a control, a corresponding volume of DMSO (solvent control) or filter control was added to the medium. If appropriate, positive and negative controls were used in the assays and they are described within each assay section. This 2D cellular model of human microglia has a short period for functional testing *in vitro* and thus, is not suitable for long-term exposure with low exposure dose. Due to this, short and high-dose exposure have been used to bring forth possible impact which can be studied further in more suitable models.

3.2. Particle collection and characterization

In this study, we used three diesel-derived pollutant particles, named A20, A0 and E6. The particles were collected at VTT Technical Research Centre of Finland Ltd. and analyzed and characterized previously (Hakkarainen et al., 2023; Mussalo et al., 2023; Saarikoski et al., 2024). Briefly: A0 and A20 particles were collected from the exhaust of a heavy-duty diesel engine, which was a modern 4-cylinder 4.4 dm^3 turbocharged diesel unit equipped with high-pressure common-rail fuel injection without any exhaust after-treatment device. E6 was collected from the exhaust of a 2019 model diesel car, with a 1.6 dm^3 turbocharged engine and Euro 6d-TEMP emission rating and Diesel Particulate Filter (DPF) and Selective Catalytic Reduction (SCR) after-treatment device.

For A20, the engine was run with regular petroleum diesel, which meets the EN590 specifications and with an aromatic content of 20 wt-% and fatty acid methyl ester (FAME) content <0.1 vol-%. A0 was collected from paraffinic renewable diesel (Neste renewable diesel, made from feedstocks) with an aromatic content of 0.1 % and FAME content <0.1 %. In addition, the same renewable diesel was used for the modern diesel car (E6). Both fuels were provided by Neste Oyj (Espoo, Finland). The engine (for A20 and A0) was run on an electrical dynamometer according to the ISO 8178 RMC-C1 test cycle. The car (for E6) was driven on a light-duty chassis dynamometer according to the Worldwide Harmonized Light Duty Test Cycle (WLTC).

For the A20 and A0, the particles were collected from the exhaust with a diluting sampling system (SPC472 Smart Sampler, AVL List GmbH, Graz, Austria) according to the ISO 8178 standard. For E6, raw exhaust from the car was a Constant Volume Sampler (CVS)-type dilution tunnel. In all cases, particles were collected on a fluorocarbon membrane filter (Fluoropore, Merck KGaA, Darmstadt, Germany), which were methanol-washed, dried, and weighed. After exhaust collection, to determine the particle mass, filters were weighed again and stored at −20 °C until extraction of the particles.

3.3. Particle composition

The particle composition of the pollutants has been previously described (Hakkarainen et al., 2023; Mussalo et al., 2023; Saarikoski et al., 2024). To summarize: commonly used characterization of the content of metals, polycyclic aromatic hydrocarbons (PAH), and carbon in the particulate matter was done and the main findings are summarized in (Table 1). A20 and A0 contained a significantly higher number of particles compared to E6. The size of the particles was in the range of ultrafine particles (<100 nm) in all used pollutants.

3.4. Particle extraction

Particles were extracted from the filters by placing the cut filters inside a glass tube containing methanol followed by 30 min sonication (temperature <30 °C). Methanol was partly evaporated with a rotary evaporator (35 °C, 150 mbar). The rest of the methanol/particle suspension was transferred to a 15 mL glass vial and the rest of the methanol was evaporated with nitrogen flow. The dry particle samples were stored at −20 °C until reconstitution. The same procedure was conducted for control filters without exposure to the diesel exhaust to produce filter controls (FC-A, FC-E).

3.5. Particle reconstitution for exposures

For the pollutant preparation, particles were brought to room temperature for 30 min before suspension to 10 % DMSO (Sigma-Aldrich) in sterile H_2O (Baxter). First, DMSO was added to the vials, which were mixed by vortexing and followed by sonication for 10 min (SilverCrest, Ultrasonic cleaner, 50 W, 50 Hz). Sterile H_2O was added, and the particles were gently suspended in the DMSO/H_2O solution with sterile and methanol-washed glass rods followed by 20 min of sonication. Prepared pollutants were aliquoted to polystyrene tubes and stored at +4 °C (2–5 days) or −20 °C. Particles were sonicated for 5 min after storage before vortexing and mixing with the culture medium. Filter controls (FC-A, FC-E) as well as solvent control (10 % DMSO in H_2O) were prepared at the same time.

3.6. Extraction and use of mouse primary microglia

C57BL/6J mice from the central animal laboratory at the University of Groningen were housed and handled according to Dutch standards and guidelines (Protocol 2215899–01-002). All experiments were approved by the University of Groningen Committee for Animal Experimentation. Primary microglia cultures were prepared from 0 to 3-day-old C57BL/6 pups as previously described (Dolga et al., 2012; Sabogal-Guáqueta et al., 2023). Briefly, brains from the pups were dissected, minced, and dissociated with 0.25 % Trypsin and DNAse for

Table 1
Summary of diesel exhaust components. The most common components present in diesel exhaust analyzed (Hakkarainen et al., 2023; Mussalo et al., 2023; Saarikoski et al., 2024).

	A20	A0	E6
Summary	Heavy-duty diesel engine, petroleum diesel (EN590)	Heavy-duty diesel engine, renewable diesel (EN15940)	2019 diesel car with aftertreatment system, renewable diesel (EN15940)
Size	<100 nm	<100 nm	<100 nm
PAH (major components)	pyrene, chrysene, phenanthrene, 1-methyl phenanthrene, fluoranthene*	pyrene, chrysene, fluoranthene, benz[*a*]anthracene, benzo[*b*]fluoranthene*	No PAHs detected
Metals (highest to lowest)	Na, Ca, Ni, P, Zn, B, Cr **	Ni, Ca, P, B, Zn, Cr **	No metals detected
Carbon	Black carbon, elemental carbon	Black carbon, elemental carbon	No black carbon

Anions (SO_4, NO_3, Cl, Br, F) below the detection limit

* 20 PAHs detected out of 24 PAHs analysed.

** Below the detection limit: Hg, Ag, Al, As, Ba, Be, Br, Cd, Co, Cu, K, Li, Mg, Mn, Mo, Pb, Rb, Sb, Se, Sn, Sr, Th, Tl, U, V.

25 min. The obtained cells were cultured in Dulbecco's modified Eagle containing (DMEM, Gibco, 42430025), supplemented with 10 % fetal bovine serum (FBS, Hyclone, SV30160), 1 mM Sodium Pyruvate (Gibco, 11360070), and 100 U/mL P/S (ThermoFisher, 15070063) at 37 °C and 5 % CO_2. After 48 h of *in vitro* cultivation, the flasks were rinsed with 3 mL of fresh medium and the growth medium was completely replaced by fresh medium. After 10–14 days, microglia were lifted in the culture medium by mechanically shaking the flasks for 60 min, at 150 rpm. Collected microglia were subcultured into uncoated well plates as per experimental requirements. The cells were maintained in a mix of 50 % astrocyte-conditioned medium and 50 % fresh DMEM, supplemented with 10 % FBS and 100 U/mL P/S. Primary microglial cells from 1st to 3rd passage were used for all the experiments.

3.7. Use and maintenance of human induced pluripotent stem cells (iPSCs)

Human iPSC lines used in this study are listed in Table 2. Informed consent was obtained from all the donors. All experiments with iPSCs and iPSC-derived cells were performed by the Declaration of Helsinki (World Medical Association, 2013), with permission from the Research Ethics Committee of the Northern Savo Hospital District (license no. 123/2016). Lines were generated upon approval from the human research ethics committees of the Royal Victorian Eye and Ear Hospital (11/1031H), University of Melbourne (1545394), University of Tasmania (H0014124), with the requirements of the National Health & Medical Research Council of Australia (MBE2968, MBE290), or upon approval of approval from the committee on Research Ethics of Northern Savo Hospital District (license no. 123/2016) (MAD1, MAD6, MAD8, CTRL8.2, LL190). BIONi037-A (RRID:CVCL_II80, Biosample ID: SAMEA104026330) and BIONi010-C-2 (RRID:CVCL_II81, Biosample ID: SAMEA4342705) lines were purchased for research use from the European Bank for Induced pluripotent stem cells (EBiSC).

iPSC cultures were maintained at +37 °C, 5 % CO_2 with atmospheric oxygen in a humified incubator, in complete Essential 8 −medium (E8, Gibco) supplemented with 0.5 % P/S (v/v, Gibco) on Matrigel-coated (Corning) dishes. The medium was changed daily, and the cells were passaged twice per week with 0.5 mM EDTA, supplementing the medium with 5 μM ROCK inhibitor (Selleckchem, S1049) for the first day. For the differentiation into iMGLs, the iPSCs were split three days before to acquire 50–70 % confluency on the D0. The cultures were tested negative for mycoplasma with Mycoalert (Lonza) before starting any differentiation.

3.8. Differentiation of iMGLs

Microglia-like cells were differentiated with our previously published protocol, a three-week protocol (Konttinen et al., 2019) with minor modifications. Briefly: on D0, differentiation was started from single-cell suspension of iPSC, which were plated on Matrigel-coated (Corning) dishes in E8 + P/S medium containing BMP4, Activin A (both Peprotech), CHIR 99021 (Axon) and ROCK and placed in hypoxic condition to induce mesodermal differentiation. The fresh medium was changed within 24 h. For D2-D8, in-house made base medium containing Glutamax, P/S (both Gibco), ascorbic acid, sodium selenite (both Sigma), and sodium bicarbonate (Gibco) in DMEM/F-12 (Gibco) was used. On D2-D3, the base medium was supplemented with FGF, VEGF (both Peprotech), insulin (Sigma) and SB431542 (Selleckchem). On D4, the cells were transferred to normoxia in a base medium supplemented with FGF, VEGF, TPO, SCF, IL-3, IL-6 (all Peprotech), and insulin and maintained with daily medium changes until D8. Floating progenitors were collected on D8 and seeded on ultra-low attachment culture vessels (Corning) in medium containing IL-34, MCSF (both Peprotech), and insulin in base-medium composed of IMDM, in-house heat-inactivated FBS (iFBS) and P/S (all Gibco). For the rest of the differentiation, IMDM, iFBS, and P/S containing medium was supplemented with only IL-34 and MCSF. At D16, the cells were seeded on experiment plates and let to mature until experiments with half medium changed every day. Experiments were conducted between D20-D24. Details on the cell density and plate formats are listed in Table 3.

3.9. Evaluation of pollutant exposure to cell viability (multiple concentrations)

To investigate if the pollutants are cytotoxic for the iMGLs, the cytotoxicity of different concentrations of the pollutants was evaluated. For A0, tested concentrations were 26.5, 66.25, 132.5, and 265 μg/mL. To collect 1 mg of A0, 558 L of exhaust was run through the collection filter (Mussalo et al., 2024). Thus, these A0 concentrations correspond to 15, 37, 74, and 148 L/mL as a dose of emission volume. For A20, 17.9, 44.75, 89.5, 179 μg/mL. For A20, to collect 1 mg of particles, 337 L of exhaust was run through the filter. These A20 correspond to 7, 17, 34, and 67 L/mL. As E6 did not contain a comparable mass of particles, the exhaust amount was calculated as the volume of exhaust run through the filter. For cytotoxicity testing, 12.5, 25, 50, 100, and 125 L of exhaust/mL (L/mL) were used. Controls consisted of corresponding concentrations of DMSO (Table 4.) In addition, one concentration of filter control (FC-A) was used. To induce certain cell death, iMGLs were exposed to a high concentration of DMSO (50 %).

Live-cell cytotoxicity measurement: To assess the cytotoxicity of the pollutant exposure over time, Cytotox Green (4633, Essen Bioscience Ltd., United Kingdom) and live-cell imaging platform, Incucyte® S3 (Sartorius, Essen BioScience) were used according to manufacturer's instructions. Pollutants or controls were administered to cells in a

Table 2
iPSC lines used in this study. Abb. = abbreviation, F = female, M = male, KO = knock-out, only one functional *APOE* allele, RNAseq = used in RNA sequencing, Func. = used in the functional testing.

Name	Abb.	F/M	Age	APOE	Karyotype	Experiments	Reference
MAD1 clone 7	M1	M	67 y	3/3	46 XY	RNAseq, Func.	(Jäntti et al., 2022)
MAD6 clone 1	M6	M	63 y	3/3	46 XY	RNAseq, Func.	(Fagerlund et al., 2021)
MAD8 clone 1	M8	M	64 y	3/3	46 XY	RNAseq, Func.	(Jäntti et al., 2022)
MBE2960 clone 1	MB60	M	78 y	3/3	46 XY	RNAseq	(Muñoz et al., 2020)
MBE2968 clone 1	MB68	F	65 y	3/3	46 XX	RNAseq	(Jäntti et al., 2022)
LL190 clone 1.5	LL	F	44 y	3/3	46 XX	RNAseq	(Oksanen et al., 2017)
CTRL8.2	CTRL	F	Adult	3/3	46 XX	RNAseq	(Holmqvist et al., 2016)
BIONi037-A	BA	F	77 y	3/3	46 XX	RNAseq	(Nimsanor et al., 2016)*
BIONi010-C-2	BC2	M	18 y	3/KO	46 XY, duplication of 1,4Mbp on Chr22 in q11.23	Func.	(Schmid et al., 2020, 2019)*

* Distributed by European Bank for induced pluripotent Stem Cells (EBiSC), https://ebisc.org/.

Table 3
Details of the used iMGLs cell densities and exposure volumes per each assay. Cv = coverslip.

Assay	Format	Cells per vessel	Exp. volume (µL)	Area (cm^2)	Notes
24 h exposure					
Cytotox	96-well plate	15,000	100	0.32	
MTT and LDH assay	96-well plate	15,000	100	0.32	
	48 -well plate	30,000	250	1.1	
Immunocyto-chemistry	96-well Ibidi	25,000	200	0.56	
Ca^{2+} imaging	6 mm coverslip on a 3.5 cm dish	6,000	2,000 (per dish) 64 (per cv)	8.8 (dish) 0.28 (cv)	
RNAseq	6 cm dish	1,000,000	4,000	21.5	
Mito Stress	96-well (XFe96 plate, Agilent)	50,000	150	0.114	
Phagocytosis/ Cytokine	96-well plate (ImageLock, Sartorius)	15,000	100	0.32	without iFBS
Electron microscopy	6 mm coverslip on 12-well plate	6,000	750 (per well) 60 (per cv)	3.5 (well) 0.28 (cv)	
Acute exposure					
Scratch wound	96-well plate (ImageLock, Sartorius)	30,000	100	0.32	
Lysoview	96-well plate (Nunclon, Thermo)	15,000	100	0.32	

medium containing a 1:4000 dilution of Cytotox Green. Cells were immediately imaged with IncuCyte S3 (Sartorius), with 10X objective, phase, and green channels with default settings. The plate was imaged every 3 h, two images per well for at least 24 h. To estimate the cytotoxicity, the green fluorescence signal coming from nuclei of cells with disrupted cell membranes was analyzed with Incucyte® S3 with surface-fit segmentation. As pollutant particles might cause autofluorescence, the localization of the fluorescence in nuclei was estimated with the help of phase images. Confluency was measured with AI confluence mode.

Metabolic activity (MTT-assay): The end-point impact of multiple pollutant concentrations on the metabolic activity was evaluated with a colorimetric MTT-assay. iMGLs were seeded on a 96-well plate (15,000 cells/well). iMGLs were exposed for 60 h for A0 and A20 in the normal microglial medium. After the exposure period, 3-(4,5-dimethylthiazol-2-yl)-2,5-diphenyltetrazolium bromide MTT-reagent (Sigma) was added to cells in a final concentration of 0.5 mg/mL, and incubated with the reagent for 4 h, at + 37 °C, 5 % CO2. As a control, cell death was induced with 1 % Triton-X. The cellular conversion of the MTT-reagent to purple formazan was detected under a light microscope. The medium was removed, and cells were solubilized with DMSO (Sigma) overnight, RT. Absorbance was measured with a Victor Wallac plate reader, at 595 nm. The absorbance readings were background corrected, and the metabolic activity was calculated as fold-change over untreated (medium) iMGLs activity.

We noticed that iMGLs survival would decrease if no fresh media was added every 24 h (Jäntti et al., 2024). Due to this and the limited availability of the pollutants, the exposure time was decreased to 24 h for cytotoxicity testing of E6 and the following assays.

Table 4
Summary of the pollutant and DMSO (solvent control) concentrations tested for cytotoxicity assays. NA = not applicable.

	Pollutant dose		Final DMSO (%)	
	µg/mL	L/mL	For live-cell cytotoxicity assay	For MTT assay
A20	17.9	7	0.13	0.13
	44.8	17	0.13	0.13
	89.5	34	0.53	0.53
	179	67	0.53	0.53
A0	26.5	15	0.13	0.13
	66.3	37	0.13	0.13
	132.5	74	0.53	0.53
	265	148	0.53	0.53
Filter control	NA	NA	0.13	0.13
E6	NA	12.5	0.2	0.1
	NA	25	0.2	0.2
	NA	50	0.4	0.4
	NA	100	1.0	0.8
	NA	125	1.0	1.0
Positive control	–	–	50	50
Medium	–	–		–

3.10. Cytotoxicity assay for the final exposure concentration

One concentration of pollutants was selected for further testing. To eliminate the effect caused by different DMSO concentrations as a solvent, the stock concentration of the pollutants or filter controls was equalized to 2,000 L/mL. The test concentration of the pollutants and filter control was set to 50 L/mL (dilution factor 40). As a mass, this corresponds to the final exposure concentration for A0 as 90 µg/mL and for A20 as 132.5 µg/mL. The final DMSO concentration was 0.25 %. To confirm that this concentration is not cytotoxic, the impact on cellular metabolic activity was measured with MTT as above but using 10 % DMSO as a positive control for cell death. In addition, a lactate dehydrogenase (LDH) release assay was used.

Release of LDH: possible disruption of the cell membrane due to pollutant exposure was assessed by the release of lactate dehydrogenase (LDH) using CyQUANT™ LDH Cytotoxicity Assay Kit (C20301, Invitrogen) according to manufacturer's instructions. The maximal cell lysis and acute release of LDH was induced by adding Triton-X-100 to 1 % final concentration to a quadruplicate set of wells for 5 min before starting the medium collection. The released LDH catalyzed enzymatic reactions and led to a reduction of tetrazolium salt to red formazan. The absorbance of red formazan was measured at 490 nm. For background correction, absorbance was measured at 650 nm. The percentage of LDH release was compared to absolute cell lysis induced by Triton-X-100.

3.11. Osmolality and pH of pollutant exposure

The pH of the exposure mixture was determined to be 7.4 with pH paper (109543, Millipore). The osmolality was determined to be between 332 to 348 mOsm (Pharming O4 EQ-ANL-03A-006 osmometer) as normal culture medium was 275 mOsm. As also medium containing the solvent control (10 % DMSO in H_2O diluted to a final concentration of 0.25 % DMSO) was 337 mOsm, we concluded that the osmolality change was due to DMSO/ H_2O addition.

3.12. Immunocytochemistry for microglial markers

For immunostaining, iMGLs were seeded on a 96-well Ibidi plate, in a density of 25,000 cells/well. Microglia were exposed to pollutants for 24 h and fixed with pre-warmed, in-house made 4 % Paraformaldehyde (PFA) for 20 min, RT. After washing thrice with PBS, the iMGLs were permeabilized with 0.5 % Tween, 0.2 % Triton in 5 % normal goat serum (NGS) in PBS for 20 min followed by 2 h blocking with 0.2 % Triton in 10 % NGS in RT. The primary antibodies were added in 0.2 % Triton in 5 % NGS and incubated overnight, at +4 °C. The following dilutions of antibodies were used: 1:100 for IBA1 (019–19741, Wako), PU.1 (2266S, Cell Signalling technology), and TMEM119 (ab185333, Abcam), and dilution 1:125 was used for P2RY12 (HPA014518, Sigma-Aldrich). Negative control was incubated without primary antibody. The excess

primary antibody was washed thrice, and the secondary antibody (Alexa Fluor™ 568, A-11011, Invitrogen) was incubated at 1:500 dilution overnight +4 °C. The secondary antibody was washed three times with PBS and the nuclei were counterstained with bizbenzimide for 5 min during the last wash. The samples were kept at +4 °C and filled with PBS until imaging. Staining was visualized with LSM700, AxioObserver (Carl Zeiss Microimaging GmbH, Jena, Germany) confocal microscope using EC Plan-Neofluar 10x/0.30 M27 objective, with 405/435 nm (blue) laser for nuclei, 555/573 nm (red) for marker staining. Z-stack images were acquired with 2 μm intervals. The maximum intensity projection in Zen Black (Carl Zeizz) was used to compose the stack images.

3.13. Intracellular Ca^{2+} −imaging

The impact of pollutants on intracellular Ca^{2+} −signaling was investigated using a Ca^{2+}-sensitive Fluo-4 dye (F10471, Invitrogen). iMGLs were seeded on 6 mm coverslips, 6,000 cells/coverslip. iMGLs were exposed to pollutants for 24 h. The Ca^{2+} −imaging was performed as described previously (Konttinen et al., 2019). Shortly: after pollutants exposure, the iMGLs were loaded with Fluo-4 dye for 30 min at +37 °C followed by washing with a basic solution. The intracellular Ca^{2+} responses to 5 sec application of 100 μM ATP or ADP (Sigma) were measured with the TILL photonics imaging system (TILL Photonics GmbH, Germany). Fluorescence of the Fluo-4 (monochromatic light 495/506 nm) was visualized with a 10X objective in an Olympus IX-70 microscope (Tokyo, Japan) with CCD camera (SensiCam, PCO imaging, Kelheim, Germany). Exposure time was set to 100 ms and one frame per second was acquired. The amplitude of Ca^{2+} transients caused by ATP or ADP application was calculated by normalizing the peak amplitude to baseline. The data was pre-analyzed using ImageJ (Rasband, W.S., ImageJ, U.S.National Institutes of Health, Bethesda, Maryland, USA, https://imagej.nih.gov/ij/), and results were obtained via Origin 2019b (OriginLab, Northampton, Massachusetts, USA).

3.14. RNA extraction and sample preparation for sequencing

For RNA collectiin, iMGLs were seeded on 6 cm dishes, 1 million cells/dish. iMGLs were exposed to pollutants for 24 h. As a positive control, iMGLs were stimulated with 20 ng/mL LPS (serotype 0111:B4, L2630, Sigma-Aldrich) to induce a strong inflammatory response. In addition, 0.25 % DMSO was used as solvent control. After exposure, cells were washed with ice-cold PBS twice and the dry plates were immediately placed on dry ice. The cells were collected using Trizol Reagent (Invitrogen #15596018) and stored at −70 °C until RNA extraction.

The RNA was extracted according to the Trizol Reagent extraction protocol. Briefly: 0.2 mL of chloroform was mixed with the sample and incubated 5 min RT followed by centrifugation (15 min, 13,000 × g, +4 °C). The colorless upper aqueous phase containing the RNA was collected. To precipitate the RNA, 0.5 mL of isopropanol was added followed by mixing and incubation for 10 min, RT. Samples were centrifuged (10 min, 13,000 × g, +4 °C). The supernatant was discarded, and the RNA was washed twice with 75 % ethanol with centrifugation (5 min, 7,500 × g, +4 °C) in between. The supernatant was removed, and samples were air-dried. Pellets were suspended to 40 μL of nuclease-free H_2O with 1 μL of RiboLock RNase Inhibitor (Thermo Scientific). RNA concentration was measured with NanoDrop (Thermo Fisher Scientific, Hudson, NH). The RNA samples were purified using an RNA clean and concentrator kit (Zymo Research, Irvine, CA, USA) with DNAse treatment before the column purification according to the manufacturer's instructions. The RNA integrity (RIN-value) was measured using an RNA Nano 6000 −kit and Bioanalyzer 2100 (both Agilent, Santa Clara, CA, USA). All the samples had RIN-values above 6, and most samples >8.

In addition, RNA was extracted from mouse primary microglia exposed to A20, A0, or 0.25 % DMSO (as a vehicle) for 24 h. The mouse microglia were seeded on a 6-well plate with a density of 450 000 cells/well and cultivated for 48 h before exposure and RNA samples were collected similarly as iMGLs samples.

3.15. RNAseq library preparation

For RNA samples from iMGLs, RNA concentrations were determined utilizing the Qubit™ 4 fluorometer (Invitrogen) and Qubit™ RNA HS kit (Thermo Fisher Scientific). The removal of ribosomal RNA was accomplished using the NEBNext® rRNA Depletion Kit v2 (Human/Mouse/Rat) (New England BioLabs, Ipswich, MA, USA). cDNA libraries were prepared employing the NEBNext® Ultra™ II Directional RNA Library Prep Kit for Illumina® (New England BioLabs). Purification and size-selection steps were performed with SPRi beads (Beckman Coulter Inc). Libraries were quantified using a high-sensitivity dsDNA Kit (Thermo Fisher Scientific) on a Qubit fluorometer (Invitrogen). A Fragment Analyzer and High Sensitivity NGS Fragment Analysis Kit (1–6000 bp) (both Agilent) were employed to assess the fragment size distribution of the libraries. Finally, the libraries were sequenced (2 × 100 cycles, paired-end) on the Illumina NovaSeq 6000 platform using NovaSeq 6000 S1 Reagent Kit v1.5 (200 cycles) (Illumina, San Diego, CA, USA).

The RNA samples from primary mouse microglia were sequenced at Biomarker Technologies (BMKGENE, Germany). Samples were prepared using Illumina Stranded mRNA-Seq (polyA enriched, strand-specific library) and libraries were sequenced (PE150 sequencing strategy, 25 M reads) using NovaSeq × Plus (Illumina).

3.16. RNAseq data analysis

RNAseq analysis was carried out as published previously (Ohtonen et al., 2023). Reads were aligned to the human reference genome GRCh38 (human iMGLs) or mouse reference genome GRCm39 (mouse primary microglia). For quality control, the features of the samples were investigated with unsupervised clustering (Gu et al., 2021) and similarity analysis and multi-dimensional scaling analysis based on the measure developed in StellarPath (Giudice et al., 2024). No batch effect was observed in the data. Cell-type specific marker signatures were collected from PanglaoDB (Franzén et al., 2019). Differential expression analysis was performed using limma and edgeR workflow (Law et al., 2018). Functional enrichment analysis of differentially expressed genes was analyzed with QIAGEN Ingenuity Pathway Analysis (IPA, QIAGEN Inc., https://digitalinsights.qiagen.com/IPA) with default parameters and human annotation (Krämer et al., 2014).

3.17. iMGLs functional testing

For the functional testing, the live-cell imaging instrument, Incucyte® S3 (Sartorius, Essen BioScience Ltd., United Kingdom) with software versions 2021C and 2022B was used. Images were acquired with default settings if not stated otherwise.

3.18. Phagocytosis assay

For the phagocytosis assay, iMGLs were seeded on ImageLock-plate (BA-04856, Sartorius), 15,000 cells/well. The iMGLs were exposed to pollutants for 24 h. For the assay and exposure, iFBS was omitted from the medium. The pHrodo™ Green Zymosan BioParticles™ (P35365, Invitrogen) were suspended in OPTI-MEM (31985047, Gibco) and sonicated for 5 min. Before adding the bioparticles, the plate was imaged once with Incucyte® S3 to measure the confluence in each well. 75 μL of medium was collected from the cells and bioparticles were added to (6.7 μg of bioparticles/well). Immediately, the plate was placed back to IncuCyte and imaging started. The plate was imaged with 10X objective, with phase and green channels with default settings, 1 image/well. Phagocytosis was assessed for 6 h, image was taken every 30 min. For each pollutant treatment, only OPTI-MEM without bioparticles was

added for controlling the background in analysis. The fluorescence produced from internalized bioparticles was quantified with Incucyte® S3 Software using the surface-fit fluorescence segmentation program. The green calibrated units for each well were normalized to cell confluency before the addition of the bioparticles.

3.19. Cytokine expression and release

The RNAseq data was used to assess the expression of cytokine and chemokine genes. For visualization, the $\log_2$CPM values of significantly differentially expressed cytokine and chemokine genes were transformed to z-score. To study the release and secretion of the cytokines into the culture medium, iMGLs were exposed to particles for 24 h in a medium without serum with 15,000 cells/well in a 96-well plate. In addition, each pollutant mixture was added to wells without cells to assess if the pollutants cause any background. The medium was collected and centrifuged (1,200 g, for 5 min). The medium samples from six wells were pooled and transferred immediately to storage at −70 °C.

The cytokine and chemokine concentrations in the medium samples were measured with BD™ Cytometric Bead Array (CBA) Human Soluble Protein Master Buffer Kit (BD Biosciences). The CBA assay was performed according to the manufactureŕs instructions. Following bead array flex sets were used (all BD Biosciences): TNFα (position C4), IL-8 (position A9), IL-10 (position B7), IL-1β (position B4), MIP-1α (position B9) and IL-6 (position A7). Standards and undiluted samples were pipetted in a round-bottom 96-well plate and incubated with 75X dilutions with bead mixture followed by 75X dilution of detection mixture. Four technical replicates were used for each sample. After washing, samples were run on Cytoflex S (Beckman Coulter). A red laser (638 nm) was used for excitation and the bead clusters were detected with 660/20 BP (APC channel) and 780/60 BP filters (APC-A750 channel). The reporter PE was excited with a yellow laser (561 nm) and detected with filter 585/42 BP. At least 400 events for each bead population were recorded. The data was analyzed with FCAP array 2.0 (SoftFlow) and cytokine and chemokine concentrations were calculated from medium samples using the known standards. For normalization, the total protein concentration of the medium samples was measured using the Bradford-based protein assay (500–0006, Bio-Rad).

Background samples with only pollutants exhibited similar absorbance values in protein measurement as the plain medium. For CBA, the PE fluorescence was at a similar level as the zero standard for each analyte (no detection of cytokines or chemokines in the sample). IL1β was only detected from the samples from one genotype (MAD6). TNFα was not detected in any samples from one genotype (MAD8). In the case of IL10, some pollutant-exposed samples were under the limit of detection (LOD). For statistical testing, these samples were given the value of LOD (specific for IL-10) divided by 2 (half of LOD).

3.20. Mitochondrial functions via Mito Stress test

The impact of the pollution on the mitochondrial respiration of iMGLs was measured with the Mito Stress assay (Agilent) according to the manufactureŕs instructions. 50,000 iMGLs/well were seeded Seahorse XFe96-well plate (XFe96 FluxPak, 102416–100, Agilent). The iMGLs were exposed to pollutants for 24 h. The XF assay medium pH 7.4 (103575–100, Agilent) was supplemented with a final concentration of 25 mM glucose (Sigma), 2 mM L-glutamine, and 1 mM sodium pyruvate (both Gibco). The Mito Stress assay was run according to the manufacturer's instructions. The oxygen consumption rate (OCR) was measured with the Seahorse XFe96 analyzer (Agilent) in response to injections of 1. Oligomycin 2.) Carbonyl cyanide 4-(trifluoromethoxy)phenylhydrazone (FCCP) 3.) Rotenone and Antimycin A (all Sigma). The final concentration of the reagents on the cells was 1 μM. After the assay, the plate was washed once with PBS and the protein amount per well was measured with Pierce™ BCA Protein Assay Kit (Thermo Scientific) for normalization.

The data was analyzed with the XF Cell Mito Stress Test Report Generator (Agilent) according to the manufacturer's instructions. Before analysis, the OCR for each well was checked. Technical replicate was excluded from the analysis if a response to any of the injections was missing or it produced negative OCR readings.

3.21. Scratch wound assay

Cells were seeded on ImageLock plate, 30,000 cells/well to obtain a confluent monolayer of cells. The layer of the cells was scratched with the Wound Maker (Sartorius, IncuCyte® Scratch Wound Assay) according to the manufactureŕs instructions to create an even wound in the cell layer. Movement of iMGLs was assessed in the presence of the pollutants with or without 100 μM adenosine-diphosphate (ADP, Sigma). The plate was imaged every 30–60 min, 10X objective, and phase channel. The relative wound density (RWD) was used to estimate the movement of the iMGLs in the presence of the pollutants.

3.22. Lysosome functions

Cells were seeded on a 96-well Nunclon plate (Thermo Scientific), 15,000 cells/well. The impact of particles on lysosomal dynamics was investigated with live-cell imaging. Lysosomal dye Lysoview 540 (1X, Biotium, 70061) was loaded in iMGLs according to the manufactureŕs instructions in the microglial medium and incubated for 30 min, +37 °C, 5 % CO_2. The iMGLs were imaged with the IncuCyte S3, at 20 min timepoint for timepoint zero reading (T_0). Treatments or pollutants were added to a final concentration of 50 L/mL. The plate was imaged every 2 h, for 24 h, with 10X objective and phase and red fluorescent channels. The exposure time for the red channel was set to 450 ms. For negative control, 5 mM NH_4Cl was included in the assay medium to increase lysosomal pH. For positive control, a medium without FBS was included to increase lysosomal staining via induction of autophagic processes. The fluorescence of the Lysoview located in acidic organelles was analyzed with surface fit-fluorescence segmentation. The fluorescence values (red calibrated unit, RCU) were normalized by setting T_0 fluorescence to 100 %. For mouse primary microglia, cells were seeded in 96-well plates with a density of 15,000 cells/well and cultured for 48 h. Similarly to iMGLs, cells were stained with 1X Lysoview 540 (Biotium) and lysosomal dynamics were imaged with live-cell imaging on IncuCyte S3. The primary microglia were exposed to A20 or A0, and 0.25 % DMSO was used as vehicle condition. The changes in Lysoview intensity were analyzed similarly to iMGLs.

For higher resolution imaging, the cells were seeded on a 96-well Ibidi plate, 25,000 cells/well. iMGLs were stained with Lysoview 488 or Lysoview 540 (Biotium) or with a combination of both in OPTI-MEM (31985047, Gibco) and incubated 30 min, +37 °C, 5 % CO_2. The air pollutants were added to wells and incubation was continued for 2 h. Staining was visualized with LSM800, AxioObserver (Carl Zeiss Microimaging GmbH, Jena, Germany) confocal microscope using Plan-Apochromat 40x/1.3 Oil DIC (UV) VIS-IR M27 objective, with 493/517 nm (green) laser for Lysoview 488, 557/572 nm (orange) for Lysoview 540 staining. The microscope incubator was set to +37 °C and 5 % CO_2. Single-dye-stained controls were used for setting the laser and0 gain. For z-stacks, images were acquired with 1 μm intervals. Turquoise color was used for Lysoview 488 and orange for Lysoview 540 for visualization. The brightness was adjusted in Zen Blue (Carl Zeizz) before the z-stacks were combined with maximum intensity projection in Zen Black (Carl Zeiss).

3.23. Serial block face scanning electron microscopy (SBF-SEM)

The impact of pollutants on intracellular structures was evaluated with 3D scanning electron microscopy. The iMGLs were seeded on coverslips, 6,000 cells/coverslips. IMGLs were exposed for 24 h to the

particles followed by fixation with 2.5 % glutaraldehyde, and 2.0 % paraformaldehyde (PFA) in 0.15 M cacodylate buffer supplemented with 2 mM $CaCl_2$, pH 7.4 for 30 min in RT. Coverslips were washed and shipped in a storage buffer consisting of 2 % PFA in 0.15 M cacodylate buffer with 2 mM $CaCl_2$, pH 7.4 for processing.

The samples were prepared using an adapted National Center for Microscopy and Imaging protocol (Boassa et al., 2022). The samples were postfixed in 2 % osmium tetroxide, and 1.5 % potassium ferrocyanide in 0.1 M cacodylate buffer with 2 mM $CaCl_2$ for 1 h on ice, followed by washing three times with H_2O. Then samples were placed in freshly prepared 1 % thiocarbohydrazide solution for 10 min at RT, followed by washing. This was followed by 1 % osmium tetroxide for 30 min and washing before placing the samples in 1 % uranyl acetate overnight at +4 °C. The next day, the samples were washed and followed by *en bloc* Walton's lead aspartate staining (6.6 μg/mL of lead nitrate in 0.03 M aspartic acid, pH = 5.5) for 30 min, at +60 °C. The samples were washed and followed by dehydration with increasing ethanol concentrations: 50 %, 70 %, 96 %, 2x100%, 3 min each. The samples were finally dipped into ice-cold anhydrous acetone and embedded in Durcupan ACM resin by placing the samples in 1:1 acetone:Durcupan (without component C) mixture for 1 h, 100 % Durcupan (without C) for 2 h, 100 % Durcupan (with C) for 2 h and baked in + 60 °C, for 48 h.

The samples were imaged with 3D Serial Block Face Scanning Electron Microscopy using the Gatan 3View stage (Gatan, Pleasanton, CA, USA) on FEI Quanta 250 FEG scanning electron microscope (Thermo Fisher Scientific). The data was acquired with a voxel size of 15 × 15 × 40 nm^3 (X,Y,Z), with the voltage of 2.5 kV, spot size 3. The pressure was between 0.15 and 0.31 Torr according to sample stability. The images were processed and aligned in the Microscope Image Browser (Belevich et al., 2016) and processed in ImageJ (Rasband, W.S., ImageJ, U.S. National Institutes of Health, Bethesda, Maryland, USA, https://imagej.nih.gov/ij/).

3.24. Statistical analysis and data presentation

No power calculations were made as the amount of the pollutants was limited and this study had an explorative aim. The number of technical and biological replicates was selected according to our previous experience. For RNAseq, the number of biological replicates (iPSC lines) was prioritized over technical replicates (wells). For sequencing analysis, detailed information is provided in the RNAseq analysis section. If quantified, for functional analysis, a minimum of 3 biological replicates and 3 technical replicates per line (wells) were used for quantification. Three lines included in the RNAseq were selected for functional studies. One line, which was not included in the RNAseq, was used in the MTT and LHD cytotoxicity evaluation and lysosome and phagocytosis assay.

For functional testing, as the number of technical and biological was small, testing of data normality was not reliable. The mean of the technical replicates was calculated to present the biological replicate. As an exception, Ca^{2+} −imaging was measured from single cells providing enough data points for evaluation of the normality. Ca^{2+} −response amplitude was non-normally distributed and thus, the median of the technical replicates was calculated to present the biological replicate.

The outliers were detected from the technical replicates with Grubbs test (alpha = 0.05) if not stated otherwise. For the graphs of quantification, if the number of technical replicates was small (<30), both biological and technical replicates, and biological replicates were depicted to give a more transparent representation of the variability. The number of technical and biological replicates is given in the figure legends. The data was normalized to untreated (medium), vehicle treatment (corresponding filter-control), or zero timepoint (T0). Graph visualization and statistical testing were performed in GraphPad Prism 10 (GraphPad Software, Boston, Massachusetts, USA, https://www.graphpad.com). Paired or matched statistical testing was used to account for the measured parameters from the iMGLs differentiated from the same iPSC line. The statistical test used is defined in the figure legends. Exposures were compared to the corresponding filter or solvent control. When only one variable (exposure) was measured, one-way ANOVA with Šidák multiple correction or paired *t*-test was used. With two variables (exposure and timepoint), Two-way ANOVA with Šidák multiple correction was used. P-values less than 0.05 were considered significant.

4. Discussion

Even though the impact of air pollution on brain health is not well understood, exposure to air pollutants, such as traffic-related air pollution, has been recognized as a risk factor for neurodegenerative diseases (Livingston et al., 2020). Microglia play an important role as the first line of immune defense in the brain, and pollutants threaten proper microglial functionality. Here, we investigated the direct and acute effects of three different diesel exhaust-derived particles using an *in vitro* iMGL model. It was evident that DEP produced with older emission control technology resulted in considerable alterations at the transcriptional level and impaired lysosome and phagocytic functions of the iMGLs.

At the transcriptional level, exposure to A20 and A0 caused alterations in multiple cellular pathways. Both A20 and A0 contain black carbon and polycyclic aromatic hydrocarbons (PAHs) (Mussalo et al., 2023), which can elicit a protective response in iMGLs to metabolize and remove the foreign compounds. RNAseq analysis suggested induction of stress response in iMGLs, such as activation of ferroptosis or pyroptosis pathways. Exposure to black carbon, the main component in A20 and A0 (Hakkarainen et al., 2023), has been shown to induce genotoxic effects (Di Ianni et al., 2022) as well as PAHs are also known to be genotoxic and immunotoxic (Patel et al., 2020). PAHs and other environmental pollutants also activate cellular immune response through the activation of the aryl hydrocarbon receptor (AHR) signalling pathway (Lee et al., 2015; Vogel et al., 2020), which was also evident in the A20 and A0 exposed iMGLs. Compared to A20 and A0, the particle amount is negligible in E6, and it does not contain PAHs or black carbon. Due to this difference in the chemical properties of the particles, E6 did not induce similar transcriptional response in iMGLs.

Even though A20 and A0 exposed iMGLs showed stress response at the transcriptional level, the iMGLs were still responsive to ATP and ADP and showed no cytotoxicity. In addition, pathway analysis revealed activation of pattern-recognition receptors, TREM1 signaling, and toll-like receptor signaling. Microglia use these receptors to sense their environment and the presence of bacteria or other inflammation-inducing factors (Colonna, 2023; Fiebich et al., 2018; Li and Wu, 2021). The variety of components in the particles can act as ligands for several membrane-receptors leading to microglial recognition and activation of intracellular signaling pathways. It has been shown that in cells from human olfactory mucosa, the same A20 and A0 particles induced alterations in genes associated with inflammation and xenobiotic metabolism but also in olfactory signaling and epithelial barrier functions (Mussalo et al., 2023). In addition, E6 exposure elicited differentially expressed genes in the olfactory mucosa cells, in contrast to our findings in iMGLs. This highlights a microglia-specific response to these particles.

We observed increased expression of several cytokine and chemokine genes in response to exposure to A20 and A0. However, this effect was not replicated at the level of cytokine secretion but rather exhibited the opposite effect. LPS induced similar gene transcription of cytokines and chemokines, and we have previously reported that these iMGLs can also secrete e.g. IL-8, IL-6, IL-10, and TNFα in response to LPS (Jäntti et al., 2024; Konttinen et al., 2019; Ohtonen et al., 2023). Different types of air pollutants cause distinct changes in the secretion of microglial cytokines and chemokines, such as CCL3, IL-8, and IL-1β (Gómez-Budia et al., 2020). Microglia-cell lines have been shown to induce secretion of IL-6 and IL-8 in response to diesel particulates in a co-culture model of human brain cells (Kang et al., 2021). When cultured alone, microglial

cells exhibit different diesel particulate-induced cytokine secretion profiles compared to co-cultures with endothelial cells (Seo et al., 2023). Macrophages from pollutant particle-infested lymph nodes exhibit decreased cytokine expression (TNFα, INFα) (Ural et al., 2022). A20- and A0-exposure has been previously shown to decrease the secretion of IL-1β and TNFα in an air–liquid-interface co-culture model of human lung and monocytic cell lines (Hakkarainen et al., 2023). Taken together, A20 and A0 show a more immunosuppressive effect on cytokine secretion in our iMGLs. The intracellular membrane structures are involved in cytokine transport and secretion (Murray and Stow, 2014) and we detected alterations in the cellular ultrastructure upon A20- and A0-exposure. Disruption in the cellular vesicular system may explain the observed alterations.

The intracellular membrane structures are also linked with our most striking finding of decreased lysosomal and phagocytic function of iMGLs in response to A20 and A0 exposure. Lysosomal dysfunction is tightly linked with neurodegeneration (Udayar et al., 2022). Acidic and enzyme-packed lysosomes are a critical part of cellular autophagy as well as phagocytosis, especially in microglia. The phagocytic pathway is composed of the detection and internalization of the foreign particles, followed by the formation of an intracellular phagosome which is fused with the lysosome for final degradation (Inpanathan and Botelho, 2019). Lysosomes are also a part of cellular sensing of the digested molecules to modulate the cellular machinery. The sequencing data supports our findings as we observed inhibition of phagocytosis and autophagy pathways in both A20- and A0-exposed iMGLs. In addition, exposure to A20 led to activation of the CLEAR (Coordinated Lysosomal Expression and Regulation) pathway, which is activated through lysosomal storage (Sardiello et al., 2009). Our data is in line with the surprising general effect of different pollutants in impairing phago-lysosomal machinery: in a human monocytic cell line, exposure to particulate matter leads to reduced bioparticle phagocytosis (Ural et al., 2022) and diesel exposure to monocytic cells leads to reduced lysosomal staining (Cao et al., 2015). In T-cells, diesel particulate has been shown to induce autophagic block through an accumulation of autophagosome marker, LC3 II (Pierdominici et al., 2014). Our experimental setup hints that particle exposure impacts the pH of the phagocytic vesicles. The acidic environment ensures the optimal environment for lysosomal enzymatic activity and the pH is maintained with proton pumps (Mindell, 2012). For example, TMEM175 maintains the pH of the lysosomal lumen and extrudes protons to the cytosol in case of hyper-acidification of the lysosomal lumen (Hu et al., 2022; Wu et al., 2023). The lysosomal membrane is also packed with a plethora of different ion channels, which counteract the increasing proton concentration in the lysosomal lumen (Riederer et al., 2022). DEPs can quickly accumulate in the lysosomes of microglia, and the presence of different chemicals in the diesel exhaust could disturb the sensitive lysosomal pumps and the lysosomal balance (Nie et al., 2024). Carbon black has been shown to reduce the lysosome acidification and induce membrane permeabilization in alveolar epithelial cells (Gao et al., 2023). Heavy metals have been linked to neurodegenerative diseases. Thus, especially the presence of the metals in the exhaust pose a risk for the microglia as the excess of metals can induce alterations in the lysosomal functions (Das et al., 2025). For example, excess calcium can lead to lysosomal deacidification (Milani et al., 2023; Mustaly-Kalimi et al., 2022). However, the detailed mechanism of how DEPs alter lysosomes remains to be established. Further investigation with more delicate techniques, such as lysosomal patch clamp, could be used to elucidate the alterations in ion channel functions (Chen et al., 2017).

We investigated the human-specific response to the particles. Mouse models and microglia have been used to evaluate the effects of air pollution on microglia, and the use of animal models allows investigation of inhaled pollutants in the complex brain environment (Gómez-Budia et al., 2020). However, recent studies have identified species-specific differences between human and mouse microglia, especially in their transcriptome, metabolism, and how they sense their environment (Abels et al., 2021; Galatro et al., 2017; Sabogal-Guáqueta et al., 2023). At the transcriptional level, A20 and especially A0 induced a more pronounced response in human iMGLs compared to primary mouse microglia. This is also replicated in the findings on the lysosomal assay; A20 and A0 lead to a reduction in the lysosomal functions. However, the effect was less pronounced in mouse microglia than it was in human iMGLs. This suggests that human iMGLs may be more sensitive to pollutant exposure, highlighting the importance of air pollution studies using human-derived models. For future directions, the mechanism of action behind the impaired lyso-phagocytic pathway should be studied more in detail and in a more complex environment, such as microglia containing neuronal organoids.

In this study, we concentrated only on the direct effect of particles on the inflammatory response in microglia. However, in a whole-body system, air pollution can damage the brain also via other pathways. Pollution particles entering the central nervous system can cause direct toxicity to neurons (Liu et al., 2023; Shkirkova et al., 2022) and activate other glial cells, such as astrocytes (Kang et al., 2021). Release of soluble factors (cytokines and chemokines) from pollutant-exposed astrocytes and endothelial cells can stimulate microglia and aggravate microglia-mediated neurotoxicity (Kang et al., 2021; Seo et al., 2023). Air pollution can also cause indirect damage, such as eliciting systemic inflammation, oxidative stress, and damage to the blood–brain barrier (BBB) (Arias-Pérez et al., 2020; Calderón-Garcidueñas et al., 2008; Chen et al., 2022). In mouse models, systemic inflammation has been linked to alterations in microglial surveillance functions as well as interaction with the BBB, and increased pathophysiological changes (Cangalaya et al., 2023; Guerrero-Carrasco et al., 2024; Haruwaka et al., 2019). Diesel exhaust can reduce microglial contact with the neuro-vasculature system (Greve et al., 2020), which in turn could exacerbate the BBB damage caused by pollution (Hartz et al., 2008; Seo et al., 2023). Thus, pollution-caused microglia dysfunction may aggravate the impact induced by the other mechanisms. However, all these pathways are interlinked, and the details remain still elusive. Understanding how air pollution or diesel exhaust particles impact different cell types gives deeper insight into the pathways on how air pollution can alter brain health.

The clear strength of this study is the comparison of three different DEPs prepared and tested in the same methodological setup using iMGLs differentiated from multiple iPSC lines. Many studies rely on in-house prepared pollutant stocks, and quite commonly, only one type of diesel pollutant is used (Gómez-Budia et al., 2020). This challenges the comparison of different types of pollutants. We observed clear and distinct cellular responses to different pollutants. Particles produced with older emission control technology caused alterations in the microglial transcriptome and impaired the lysosomal and phagocytotic function. In contrast, exposure to the modern alternative, E6, did not cause any alteration in the gene expression level and only minor alterations in motility and extracellular acidification rate (ECAR). The impact runs in parallel with the cleanliness of the pollutants; A20 has the highest particle amount and contains black carbon and PAHs; A0 has a similar composition but a lower particle amount. On the contrary, E6 is extremely clean and does not contain any black carbon or PAHs (Hakkarainen et al., 2023; Mussalo et al., 2023). PAHs, black carbon, and metals in the emissions have been recognized as health risks. In addition, it has also been suggested that, for example PAHs can have synergistic toxic effects (Albarano et al., 2023; Moore et al., 2018). The focus has been on reducing these in the emissions by improving diesel fuel quality as well development of different aftertreatment systems, such as particle filtration system (Pirjola et al., 2019; Razak et al., 2021; Saarikoski et al., 2024; Wang et al., 2019). This study pinpoints that advancements in engine, fuel, and emission aftertreatment technology reduce the detrimental effects of pollutants on microglial function. Our results show that the modern emission control technologies are effective in reducing both emissions and their adverse effects. In addition, by reducing the aromatic content of the fuels, impacts on the emissions could be achieved also in older vehicles or without aftertreatment

technologies, which would improve air quality and decrease the adverse effects by exhaust emissions also for the existing older fleet of vehicles.

To summarize, the current study shows clear alterations in the transcriptional level and phago-lysosomal pathway in a human microglia model in response to diesel emissions representing older technology without particle filtration. From the point-of-view of microglia and brain health, replacing older engine and emission technologies with modern alternatives, including the reduction of fuel aromatic content, could be considered less harmful. However, to obtain a more complete picture on how traffic-related air pollution impacts brain health, more research investigating the effect of particles from different engine and fuel technologies is needed.

4.1. Limitations of the study

We acknowledge some caveats in our study. We have utilized a quite immature *in vitro* model for microglia, and the used dosage was high with a short exposure time. Microglia are extremely sensitive to environmental cues and in this context, they lack their physiological environment. However, this is one of the first studies describing the pollutant effect on iMGLs. Simpler models are commonly used to reveal the possible alterations due to treatment or exposure, and it is not possible to carry out chronic exposures. We show clear dysfunction in the lysosome/phagosome pathway, which could be studied further in microglia-containing neuronal organoids. This could explain further if the pollutants impact microglia similarly in biologically more relevant environments and if exposure leads to microglia-mediated alterations in neuronal functions.

5. Declaration of generative AI in scientific writing

During the preparation of this work, the author(s) used Microsoft Copilot to improve the coherence and structure of certain sentences. After using this tool, the author(s) reviewed and edited the content as needed and take(s) full responsibility for the content of the published article.

Credit authorship contribution statement

Sohvi Ohtonen: Conceptualization, Investigation, Formal analysis, Visualization, Methodology, Validation, Writing - original draft, Writing - review & editing. **Henna Jäntti:** Investigation, Methodology. **Luca Giudice:** Software, Investigation, Formal analysis, Data curation. **Ahmed Mohammed:** Investigation, Formal analysis, Data curation. **Anastasia Shakirzyanova:** Investigation, Formal analysis. **Táňa Závodná:** Investigation. **Ilya Belevich:** Investigation. **Hong Yan:** Investigation. **Angélica María Sabogal-Guáqueta:** Investigation. **Ashley Rillo-Albert:** Investigation. **Elisa Perciballi:** Investigation. **Daniela Ferrari:** Supervision. **Liudmila Salevela:** Investigation. **Mari-Anna Väänänen:** Investigation. **Minna-Mari Tervo:** Investigation. **Mireia Gomez-Budia:** Investigation. **Zdeněk Krejčík:** Investigation. **Päivi Aakko-Saksa:** Resources, Project administration. **Katja M. Kanninen:** Project administration, Funding acquisition, Writing - review & editing. **Jan Topinka:** Project administration, Resources, Funding acquisition, Supervision. **Jari Koistinaho:** Resources. **Šárka Lehtonen:** Resources. **Eija Jokitalo:** Supervision, Resources. **Alejandra Sierra:** Investigation, Supervision, Resources. **Martina Schmidt:** Resources, Supervision. **Amalia M. Dolga:** Resources, Supervision. **Pasi I. Jalava:** Resources, Project administration, Funding acquisition, Writing - review & editing. **Paula Korhonen:** Conceptualization, Supervision, Investigation, Writing - review & editing. **Tarja Malm:** Conceptualization, Supervision, Writing - review & editing, Project administration, Funding acquisition.

Declaration of competing interest

The authors declare that they have no known competing financial interests or personal relationships that could have appeared to influence the work reported in this paper.

Acknowledgments

We thank all the individuals for donating valuable samples and people involved in the provision and generation of iPSC lines. We thank Prof Alice Pébay (The University of Melbourne) for providing the iPSC lines MBE2960 and MBE2968. This project has received funding from the European Union's Horizon 2020 research and innovation program under grant agreement No 814978 (TUBE: Transport-derived ultrafines and the brain effects), the European Union's Horizon 2020 research and innovation programme under the Marie Skłodowska-Curie agreement No 101034307 and Research Council of Finland under grant agreement No 334800. This work was supported by the Ministry of Education, Youth and Sports of the Czech Republic (the Research Infrastructure NanoEnviCZ, LM2023066) and the European Union - European Structural and Investments Funds in the frame of Operational Programme Research Development and Education - project Pro-NanoEnviCz (Project No. CZ.02.1.01/0.0/0.0/16_013/0001821). This research has been supported by funding from Päivikki and Sakari Sohlberg Foundation. We thank the University of Eastern Finland Doctoral Programme in Molecular Medicine (DPMM).

Part of the work was carried out with the support of UEF Cell and Tissue Imaging Unit, University of Eastern Finland, Biocenter Kuopio and EuroBioimaging Finland, and *In vitro* and *ex vivo* electrophysiology core facility, University of Eastern Finland. We thank Taina Suntio and Mervi Lindman, Electron Microscopy Unit, University of Helsinki for technical assistance with EM sample preparation and Biocenter Finland for EM imaging infrastructure support. We thank Laura Mussalo for her assistance with pollutant dosing and exposure.

Appendix A. Supplementary material

Supplementary data to this article can be found online at https://doi.org/10.1016/j.envint.2025.109467.

Data availability

Data presented in this article will be available upon reasonable request. RNAseq data is deposited to Zenodo and is available upon reasonable request at DOi: 10.5281/zenodo.14631368 (Giudice and Ohtonen, 2025).

References

Abels, E.R., Nieland, L., Hickman, S., Broekman, M.L.D., Khoury, J.E., Maas, S.L.N., 2021. Comparative analysis identifies similarities between the human and murine microglial sensomes. Int. J. Mol. Sci. 22. https://doi.org/10.3390/ijms22031495.

Albarano, L., De Rosa, I., Santaniello, I., Montuori, M., Serafini, S., Toscanesi, M., Trifuoggi, M., Lofrano, G., Guida, M., Libralato, G., 2023. Synergistic, antagonistic, and additive effects of naphthalene, phenanthrene, fluoranthene and benzo(k) fluoranthene on Artemia franciscana nauplii and adult. Environ. Pollut. 335. https://doi.org/10.1016/j.envpol.2023.122286.

Arias-Pérez, R.D., Taborda, N.A., Gómez, D.M., Fredy Narvaez, J., Porras, J., Hernandez, J.C., 2020. Inflammatory effects of particulate matter air pollution. Environ. Sci. Pollut. Res. 42390–42404. https://doi.org/10.1007/s11356-020-10574-w/Published.

Belevich, I., Joensuu, M., Kumar, D., Vihinen, H., Jokitalo, E., 2016. Microscopy image browser: a platform for segmentation and analysis of multidimensional datasets. PLoS Biol. 14. https://doi.org/10.1371/journal.pbio.1002340.

Boassa, D., Deerinck, T.J., Bushong, E.A., Thor, A., Ellisman, M., 2022. Preparation of cultured cells for serial block face scanning electron microscopy (SBEM). protocols.io. https://doi.org/10.17504/protocols.io.b5naq5ae.

Bongaerts, E., Lecante, L.L., Bové, H., Roeffaers, M.B.J., Ameloot, M., Fowler, P.A., Nawrot, T.S., 2022. Maternal exposure to ambient black carbon particles and their presence in maternal and fetal circulation and organs: an analysis of two

independent population-based observational studies. Lancet Planet Health 6, e804–e811. https://doi.org/10.1016/S2542-5196(22)00200-5.
Bové, H., Bongaerts, E., Slenders, E., Bijnens, E.M., Saenen, N.D., Gyselaers, W., Van Eyken, P., Plusquin, M., Roeffaers, M.B.J., Ameloot, M., Nawrot, T.S., 2019. Ambient black carbon particles reach the fetal side of human placenta. Nat. Commun. 10. https://doi.org/10.1038/s41467-019-11654-3.
Calderón-Garcidueñas, L., Solt, A.C., Henríquez-Roldán, C., Torres-Jardón, R., Nuse, B., Herritt, L., Villarreal-Calderón, R., Osnaya, N., Stone, I., García, R., Brooks, D.M., González-Maciel, A., Reynoso-Robles, R., Delgado-Chávez, R., Reed, W., 2008. Long-term air pollution exposure is associated with neuroinflammation, an altered innate immune response, disruption of the blood-brain barrier, ultrafine particulate deposition, and accumulation of amyloid β-42 and α-synuclein in children and young adults. Toxicol. Pathol. 36, 289–310. https://doi.org/10.1177/0192623307313011.
Cangalaya, C., Wegmann, S., Sun, W., Diez, L., Gottfried, A., Richter, K., Stoyanov, S., Pakan, J., Fischer, K.D., Dityatev, A., 2023. Real-time mechanisms of exacerbated synaptic remodeling by microglia in acute models of systemic inflammation and tauopathy. Brain Behav. Immun. 110, 245–259. https://doi.org/10.1016/j.bbi.2023.02.023.
Cao, Y., Jantzen, K., Gouveia, A.C.D., Skovmand, A., Roursgaard, M., Loft, S., Møller, P., 2015. Automobile diesel exhaust particles induce lipid droplet formation in macrophages in vitro. Environ. Toxicol. Pharmacol. 40, 164–171. https://doi.org/10.1016/j.etap.2015.06.012.
Chen, C.C., Cang, C., Fenske, S., Butz, E., Chao, Y.K., Biel, M., Ren, D., Wahl-Schott, C., Grimm, C., 2017. Patch-clamp technique to characterize ion channels in enlarged individual endolysosomes. Nat. Protoc. 12, 1639–1658. https://doi.org/10.1038/nprot.2017.036.
Chen, H., Oliver, B.G., Pant, A., Olivera, A., Poronnik, P., Pollock, C.A., Saad, S., 2022. Effects of air pollution on human health – Mechanistic evidence suggested by in vitro and in vivo modelling. Environ. Res. 212. https://doi.org/10.1016/j.envres.2022.113378.
Cole, T.B., Coburn, J., Dao, K., Roqué, P., Chang, Y.C., Kalia, V., Guilarte, T.R., Dziedzic, J., Costa, L.G., 2016. Sex and genetic differences in the effects of acute diesel exhaust exposure on inflammation and oxidative stress in mouse brain. Toxicology 374, 1–9. https://doi.org/10.1016/j.tox.2016.11.010.
Colonna, M., 2023. The biology of TREM receptors. Nat. Rev. Immunol. https://doi.org/10.1038/s41577-023-00837-1.
Cristaldi, A., Fiore, M., Oliveri Conti, G., Pulvirenti, E., Favara, C., Grasso, A., Copat, C., Ferrante, M., 2022. Possible association between PM2.5 and neurodegenerative diseases: a systematic review. Environ. Res. 208. https://doi.org/10.1016/j.envres.2021.112581.
Crüts, B., van Etten, L., Törnqvist, H., Blomberg, A., Sandström, T., Mills, N.L., Borm, P. J., 2008. Exposure to diesel exhaust induces changes in EEG in human volunteers. Part. Fibre Toxicol. 5. https://doi.org/10.1186/1743-8977-5-4.
Das, S., Murumulla, L., Ghosh, P., Challa, S., 2025. Heavy metal-induced disruption of the autophagy-lysosomal pathway: implications for aging and neurodegenerative disorders. Biometals. https://doi.org/10.1007/s10534-025-00665-x.
Di Ianni, E., Jacobsen, N.R., Vogel, U.B., Møller, P., 2022. Systematic review on primary and secondary genotoxicity of carbon black nanoparticles in mammalian cells and animals. Mutat. Res. Rev. Mutat. Res. https://doi.org/10.1016/j.mrrev.2022.108441.
Dolan, M.J., Therrien, M., Jereb, S., Kamath, T., Gazestani, V., Atkeson, T., Marsh, S.E., Goeva, A., Lojek, N.M., Murphy, S., White, C.M., Joung, J., Liu, B., Limone, F., Eggan, K., Hacohen, N., Bernstein, B.E., Glass, C.K., Leinonen, V., Blurton-Jones, M., Zhang, F., Epstein, C.B., Macosko, E.Z., Stevens, B., 2023. Exposure of iPSC-derived human microglia to brain substrates enables the generation and manipulation of diverse transcriptional states in vitro. Nat. Immunol. 24, 1382–1390. https://doi.org/10.1038/s41590-023-01558-2.
Dolga, A.M., Letsche, T., Gold, M., Doti, N., Bacher, M., Chiamvimonvat, N., Dodel, R., Culmsee, C., 2012. Activation of KCNN3/SK3/KCa2.3 channels attenuates enhanced calcium influx and inflammatory cytokine production in activated microglia. Glia 60, 2050–2064. https://doi.org/10.1002/glia.22419.
Ehsanifar, M., Montazeri, Z., Taheri, M.A., Rafati, M., Behjati, M., Karimian, M., 2021. Hippocampal inflammation and oxidative stress following exposure to diesel exhaust nanoparticles in male and female mice. Neurochem. Int. 145. https://doi.org/10.1016/j.neuint.2021.104989.
Ehsanifar, M., Montazeri, Z., Zavareh, M.S., Rafati, M., Wang, J., 2023. Cognitive impairment, depressive-like behaviors and hippocampal microglia activation following exposure to air pollution nanoparticles. Environ. Sci. Pollut. Res. 30, 23527–23537. https://doi.org/10.1007/s11356-022-23882-0.
Ehsanifar, M., Yavari, Z., Rafati, M., 2022. Exposure to urban air pollution particulate matter: neurobehavioral alteration and hippocampal inflammation. Environ. Sci. Pollut. Res. 29, 50856–50866. https://doi.org/10.1007/s11356-022-19367-9.
European Environment Agency, 2023. Harm to human health from air pollution in Europe: burden of disease 2023 [WWW Document]. DOi: 10.2800/721439.
Fagerlund, I., Dougalis, A., Shakirzyanova, A., Gómez-Budia, M., Pelkonen, A., Konttinen, H., Ohtonen, S., Fazaludeen, M.F., Koskuvi, M., Kuusisto, J., Hernández, D., Pebay, A., Koistinaho, J., Rauramaa, T., Lehtonen, Š., Korhonen, P., Malm, T., 2021. Microglia-like cells promote neuronal functions in cerebral organoids. Cells 11, 124. https://doi.org/10.3390/cells11010124.
Fiebich, B.L., Batista, C.R.A., Saliba, S.W., Yousif, N.M., de Oliveira, A.C.P., 2018. Role of microglia TLRs in neurodegeneration. Front. Cell. Neurosci. 12. https://doi.org/10.3389/fncel.2018.00329.
Franzén, O., Gan, L.M., Björkegren, J.L.M., 2019. PanglaoDB: a web server for exploration of mouse and human single-cell RNA sequencing data. Database. https://doi.org/10.1093/database/baz046.
Galatro, T.F., Holtman, I.R., Lerario, A.M., Vainchtein, I.D., Brouwer, N., Sola, P.R., Veras, M.M., Pereira, T.F., Leite, R.E.P., Moller, T., Wes, P.D., Sogayar, M.C., Laman, J.D., den Dunnen, W., Pasqualucci, C.A., Oba-Shinjo, S.M., Boddeke, E.W.G. M., Marie, S.K.N., Eggen, B.J.L., 2017. Transcriptomic analysis of purified human cortical microglia reveals age-associated changes. Nat. Neurosci. 20, 1162–1171. https://doi.org/10.1038/nn.4597.
Gao, M., Ge, X., Li, Y., Zheng, G., Cai, J., Yao, J., Wang, T., Gao, Y., Yan, Y., Chen, Y., Pan, Y., Hu, P., 2023. Lysosomal dysfunction in carbon black-induced lung disorders. Sci. Total Environ. 905. https://doi.org/10.1016/j.scitotenv.2023.167200.
Gawryluk, J.R., Polombo, D.J., Curran, J., Parker, A., Carlsten, C., 2023. Brief diesel exhaust exposure acutely impairs functional brain connectivity in humans: a randomized controlled crossover study. Environ. Health 22. https://doi.org/10.1186/s12940-023-00961-4.
Giudice, L., Mohamed, A., Malm, T., 2024. StellarPath: Hierarchical-vertical multi-omics classifier synergizes stable markers and interpretable similarity networks for patient profiling. PLoS Comput. Biol. 20. https://doi.org/10.1371/journal.pcbi.1012022.
Giudice, L., Ohtonen, S., 2025. Traffic-related diesel pollution particles impair the lysosomal functions of human iPSC-derived microglia. Zenodo. https://doi.org/10.5281/zenodo.14631368.
Gómez-Budia, M., Konttinen, H., Saveleva, L., Korhonen, P., Jalava, P.I., Kanninen, K.M., Malm, T., 2020. Glial smog: Interplay between air pollution and astrocyte-microglia interactions. Neurochem. Int. 136. https://doi.org/10.1016/j.neuint.2020.104715.
Greve, H.J., Mumaw, C.L., Messenger, E.J., Kodavanti, P.R.S., Royland, J.L., Kodavanti, U.P., Block, M.L., 2020. Diesel exhaust impairs TREM2 to dysregulate neuroinflammation. J. Neuroinflammation 17. https://doi.org/10.1186/s12974-020-02017-7.
Gu, Z., Schlesner, M., Hübschmann, D., 2021. cola: an R/Bioconductor package for consensus partitioning through a general framework. Nucleic Acids Res. 49. https://doi.org/10.1093/nar/gkaa1146.
Guerrero-Carrasco, M., Targett, I., Olmos-Alonso, A., Vargas-Caballero, M., Gomez-Nicola, D., 2024. Low-grade systemic inflammation stimulates microglial turnover and accelerates the onset of Alzheimer's-like pathology. Glia 72, 1340–1355. https://doi.org/10.1002/glia.24532.
Hakkarainen, H., Järvinen, A., Lepistö, T., Salo, L., Kuittinen, N., Laakkonen, E., Yang, M., Martikainen, M.V., Saarikoski, S., Aurela, M., Barreira, L., Teinilä, K., Ihalainen, M., Aakko-Saksa, P., Timonen, H., Rönkkö, T., Jalava, P., 2023. Toxicity of exhaust emissions from high aromatic and non-aromatic diesel fuels using in vitro ALI exposure system. Sci. Total Environ. 890. https://doi.org/10.1016/j.scitotenv.2023.164215.
Hartz, A.M.S., Bauer, B., Block, M.L., Hong, J.-S., Miller, D.S., 2008. Diesel exhaust particles induce oxidative stress, proinflammatory signaling, and P-glycoprotein up-regulation at the blood-brain barrier. FASEB J. 22, 2723–2733. https://doi.org/10.1096/fj.08-106997.
Haruwaka, K., Ikegami, A., Tachibana, Y., Ohno, N., Konishi, H., Hashimoto, A., Matsumoto, M., Kato, D., Ono, R., Kiyama, H., Moorhouse, A.J., Nabekura, J., Wake, H., 2019. Dual microglia effects on blood brain barrier permeability induced by systemic inflammation. Nat. Commun. 10. https://doi.org/10.1038/s41467-019-13812-z.
Hedegaard, A., Stodolak, S., James, W.S., Cowley, S.A., 2020. Honing the double-edged sword: improving human iPSC-microglia models. Front. Immunol. https://doi.org/10.3389/fimmu.2020.614972.
Holmqvist, S., Lehtonen, S., Chumarina, M., Puttonen, K.A., Azevedo, C., Lebedeva, O., Ruponen, M., Oksanen, M., Djelloul, M., Collin, A., Goldwurm, S., Meyer, M., Lagarkova, M., Kiselev, S., Koistinaho, J., Roybon, L., 2016. Creation of a library of induced pluripotent stem cells from Parkinsonian patients. NPJ Parkinsons Dis 2, 16009. https://doi.org/10.1038/npjparkd.2016.9.
Hu, M., Li, P., Wang, C., Feng, X., Geng, Q., Chen, W., Marthi, M., Zhang, W., Gao, C., Reid, W., Swanson, J., Du, W., Hume, R.I., Xu, H., 2022. Parkinson's disease-risk protein TMEM175 is a proton-activated proton channel in lysosomes. Cell 185, 2292–2308.e20. https://doi.org/10.1016/j.cell.2022.05.021.
Inpanathan, S., Botelho, R.J., 2019. The lysosome signaling platform: adapting with the Times. Front. Cell Dev. Biol. 7. https://doi.org/10.3389/fcell.2019.00113.
Jäntti, H., Jonk, S., Gómez Budia, M., Ohtonen, S., Fagerlund, I., Fazaludeen, M.F., Aakko-Saksa, P., Pebay, A., Lehtonen, Š., Koistinaho, J., Kanninen, K.M., Jalava, P.I., Malm, T., Korhonen, P., 2024. Particulate matter from car exhaust alters function of human iPSC-derived microglia. Part. Fibre Toxicol. 21, 6. https://doi.org/10.1186/s12989-024-00564-y.
Jäntti, H., Sitnikova, V., Ishchenko, Y., Shakirzyanova, A., Giudice, L., Ugidos, I.F., Gómez-Budia, M., Korvenlaita, N., Ohtonen, S., Belaya, I., Fazaludeen, F., Mikhailov, N., Gotkiewicz, M., Ketola, K., Lehtonen, Š., Koistinaho, J., Kanninen, K. M., Hernández, D., Pébay, A., Giugno, R., Korhonen, P., Giniatullin, R., Malm, T., 2022. Microglial amyloid beta clearance is driven by PIEZO1 channels. J. Neuroinflammation 19. https://doi.org/10.1186/s12974-022-02486-y.
Kang, Y.J., Tan, H.Y., Lee, C.Y., Cho, H., 2021. An air particulate pollutant induces neuroinflammation and neurodegeneration in human brain models. Adv. Sci. 8. https://doi.org/10.1002/advs.202101251.
Konttinen, H., Cabral-da-Silva, M.E.C.E.C., Ohtonen, S., Wojciechowski, S., Shakirzyanova, A., Caligola, S., Giugno, R., Ishchenko, Y., Hernández, D., Fazaludeen, M.F.F., Eamen, S., Budia, M.G.G., Fagerlund, I., Scoyni, F., Korhonen, P., Huber, N., Haapasalo, A., Hewitt, A.W.W., Vickers, J., Smith, G.C.C., Oksanen, M., Graff, C., Kanninen, K.M.M., Lehtonen, S., Propson, N., Schwartz, M.P.P., Pébay, A., Koistinaho, J., Ooi, L., Malm, T., Hernandez, D., Fazaludeen, M.F.F., Eamen, S., Budia, M.G.G., Fagerlund, I., Scoyni, F., Korhonen, P., Huber, N., Haapasalo, A., Hewitt, A.W.W., Vickers, J., Smith, G.C.C., Oksanen, M., Graff, C., Kanninen, K.M. M., Lehtonen, S., Propson, N., Schwartz, M.P.P., Pebay, A., Koistinaho, J., Ooi, L., Malm, T., Hernández, D., Fazaludeen, M.F.F., Eamen, S., Budia, M.G.G.,

Fagerlund, I., Scoyni, F., Korhonen, P., Huber, N., Haapasalo, A., Hewitt, A.W.W., Vickers, J., Smith, G.C.C., Oksanen, M., Graff, C., Kanninen, K.M.M., Lehtonen, S., Propson, N., Schwartz, M.P.P., Pébay, A., Koistinaho, J., Ooi, L., Malm, T., 2019. PSEN1DeltaE9, APPswe, and APOE4 confer disparate phenotypes in human iPSC-derived microglia. Stem Cell Rep. 13, 669–683. https://doi.org/10.1016/j.stemcr.2019.08.004.

Krämer, A., Green, J., Pollard, J., Tugendreich, S., 2014. Causal analysis approaches in ingenuity pathway analysis. Bioinformatics 30. https://doi.org/10.1093/bioinformatics/btt703.

Kwon, H.S., Ryu, M.H., Carlsten, C., 2020. Ultrafine particles: unique physicochemical properties relevant to health and disease. Exp. Mol. Med. https://doi.org/10.1038/s12276-020-0405-1.

Law, C.W., Alhamdoosh, M., Su, S., Dong, X., Tian, L., Smyth, G.K., Ritchie, M.E., 2018. RNA-seq analysis is easy as 1-2-3 with limma, Glimma and edgeR [version 3; peer review: 3 approved]. F1000Res 5. DOi: 10.12688/f1000research.9005.3.

Lee, Y.H., Lin, C.H., Hsu, P.C., Sun, Y.Y., Huang, Y.J., Zhuo, J.H., Wang, C.Y., Gan, Y.L., Hung, C.C., Kuan, C.Y., Shie, F.S., 2015. Aryl hydrocarbon receptor mediates both proinflammatory and anti-inflammatory effects in lipopolysaccharide-activated microglia. Glia 63, 1138–1154. https://doi.org/10.1002/glia.22805.

Li, D., Wu, M., 2021. Pattern recognition receptors in health and diseases. Signal Transduct. Target. Ther. https://doi.org/10.1038/s41392-021-00687-0.

Li, X., Zhang, Y., Li, B., Yang, H., Cui, J., Li, X., Zhang, X., Sun, H., Meng, Q., Wu, S., Li, S., Wang, J., Aschner, M., Chen, R., 2020. Activation of NLRP3 in microglia exacerbates diesel exhaust particles-induced impairment in learning and memory in mice. Environ. Int. 136. https://doi.org/10.1016/j.envint.2020.105487.

Liati, A., Schreiber, D., Dasilva, A.R., Dimopoulos, Y., Eggenschwiler, P., 2018. Ultrafine particle emissions from modern Gasoline and Diesel vehicles: an electron microscopic perspective. Environ. Pollut. 239, 661–669. https://doi.org/10.1016/j.envpol.2018.04.081.

Liu, F., Liu, C., Liu, Y., Wang, J., Wang, Y., Yan, B., 2023. Neurotoxicity of the air-borne particles: from molecular events to human diseases. J. Hazard. Mater. https://doi.org/10.1016/j.jhazmat.2023.131827.

Livingston, G., Huntley, J., Sommerlad, A., Ames, D., Ballard, C., Banerjee, S., Brayne, C., Burns, A., Cohen-Mansfield, J., Cooper, C., Costafreda, S.G., Dias, A., Fox, N., Gitlin, L.N., Howard, R., Kales, H.C., Kivimäki, M., Larson, E.B., Ogunniyi, A., Orgeta, V., Ritchie, K., Rockwood, K., Sampson, E.L., Samus, Q., Schneider, L.S., Selbæk, G., Teri, L., Mukadam, N., 2020. Dementia prevention, intervention, and care: 2020 report of the Lancet Commission. Lancet 396, 413–446. https://doi.org/10.1016/S0140-6736(20)30367-6.

Lloyd, A.F., Martinez-Muriana, A., Davis, E., Daniels, M.J.D., Hou, P., Mancuso, R., Brenes, A.J., Sinclair, L.V., Geric, I., Snellinx, A., Craessaerts, K., Theys, T., Fiers, M., De Strooper, B., Howden, A.J.M., 2024. Deep proteomic analysis of microglia reveals fundamental biological differences between model systems. Cell Rep. 43, 114908. https://doi.org/10.1016/j.celrep.2024.114908.

Lu, D., Luo, Q., Chen, R., Zhuansun, Y., Jiang, J., Wang, W., Yang, X., Zhang, L., Liu, X., Li, F., Liu, Q., Jiang, G., 2020. Chemical multi-fingerprinting of exogenous ultrafine particles in human serum and pleural effusion. Nat. Commun. 11. https://doi.org/10.1038/s41467-020-16427-x.

Maher, B.A., Ahmed, I.A.M., Karloukovski, V., MacLaren, D.A., Foulds, P.G., Allsop, D., Mann, D.M.A., Torres-Jardón, R., Calderon-Garciduenas, L., 2016. Magnetite pollution nanoparticles in the human brain. PNAS 113, 10797–10801. https://doi.org/10.1073/pnas.1605941113.

Milani, M., Pihán, P., Hetz, C., 2023. Calcium signaling in lysosome-dependent cell death. Cell Calcium 113. https://doi.org/10.1016/j.ceca.2023.102751.

Mindell, J.A., 2012. Lysosomal acidification mechanisms. Annu. Rev. Physiol. 74, 69–86. https://doi.org/10.1146/annurev-physiol-012110-142317.

Moore, M.N., Wedderburn, R.J., Clarke, K.R., McFadzen, I.R.B., Lowe, D.M., Readman, J. W., 2018. Emergent synergistic lysosomal toxicity of chemical mixtures in molluscan blood cells (hemocytes). Environ. Pollut. 235. https://doi.org/10.1016/j.envpol.2018.01.019.

Muñoz, S.S., Engel, M., Balez, R., Do-Ha, D., Cabral-da-Silva, M.C., Hernández, D., Berg, T., Fifita, J.A., Grima, N., Yang, S., Blair, I.P., Nicholson, G., Cook, A.L., Hewitt, A.W., Pébay, A., Ooi, L., 2020. A simple differentiation protocol for generation of induced pluripotent stem cell-derived basal forebrain-like cholinergic neurons for Alzheimer's disease and frontotemporal dementia disease modelling. Cells 9. https://doi.org/10.3390/cells9092018.

Murray, R.Z., Stow, J.L., 2014. Cytokine secretion in macrophages: SNAREs, Rabs, and membrane trafficking. Front. Immunol. 5. https://doi.org/10.3389/fimmu.2014.00538.

Mussalo, L., Avesani, S., Shahbaz, M.A., Závodná, T., Saveleva, L., Järvinen, A., Lampinen, R., Belaya, I., Krejčík, Z., Ivanova, M., Hakkarainen, H., Kalapudas, J., Penttilä, E., Löppönen, H., Koivisto, A.M., Malm, T., Topinka, J., Giugno, R., Aakko-Saksa, P., Chew, S., Rönkkö, T., Jalava, P., Kanninen, K.M., 2023. Emissions from modern engines induce distinct effects in human olfactory mucosa cells, depending on fuel and aftertreatment. Sci. Total Environ. 905, 167038. https://doi.org/10.1016/j.scitotenv.2023.167038.

Mussalo, L., Lampinen, R., Avesani, S., Závodná, T., Krejčík, Z., Kalapudas, J., Penttilä, E., Löppönen, H., Koivisto, A.M., Malm, T., Topinka, J., Giugno, R., Jalava, P., Kanninen, K.M., 2024. Traffic-related ultrafine particles impair mitochondrial functions in human olfactory mucosa cells – Implications for Alzheimer's disease. Redox Biol. 75. https://doi.org/10.1016/j.redox.2024.103272.

Mustaly-Kalimi, S., Gallegos, W., Marr, R.A., Gilman-Sachs, A., Peterson, D.A., Sekler, I., Stutzmann, G.E., 2022. Protein mishandling and impaired lysosomal proteolysis generated through calcium dysregulation in Alzheimer's disease. PNAS 119. https://doi.org/10.1073/pnas.2211999119.

Nie, B., Liu, X., Lei, C., Liang, X., Zhang, D., Zhang, J., 2024. The role of lysosomes in airborne particulate matter-induced pulmonary toxicity. Sci. Total Environ. 919. https://doi.org/10.1016/j.scitotenv.2024.170893.

Nimsanor, N., Jørring, I., Rasmussen, M.A., Clausen, C., Mau-Holzmann, U.A., Bus, C., Hoffmann, S.A., Gasser, T., Kluba, T., Holst, B., Schmid, B., 2016. Generation of induced pluripotent stem cells derived from a 77-year-old healthy woman as control for age related diseases. Stem Cell Res. 17, 550–552. https://doi.org/10.1016/j.scr.2016.09.019.

Ohtonen, S., Giudice, L., Jäntti, H., Fazaludeen, M.F., Shakirzyanova, A., Gómez-Budia, M., Välimäki, N.N., Niskanen, J., Korvenlaita, N., Fagerlund, I., Koistinaho, J., Amiry-Moghaddam, M., Savchenko, E., Roybon, L., Lehtonen, Š., Korhonen, P., Malm, T., 2023. Human iPSC-derived microglia carrying the LRRK2-G2019S mutation show a Parkinson's disease related transcriptional profile and function. Sci. Rep. 13. https://doi.org/10.1038/s41598-023-49294-9.

Oksanen, M., Petersen, A.J., Naumenko, N., Puttonen, K., Lehtonen, Š., Gubert Olivé, M., Shakirzyanova, A., Leskelä, S., Sarajärvi, T., Viitanen, M., Rinne, J.O., Hiltunen, M., Haapasalo, A., Giniatullin, R., Tavi, P., Zhang, S.C., Kanninen, K.M., Hämäläinen, R. H., Koistinaho, J., 2017. PSEN1 Mutant iPSC-derived model reveals severe astrocyte pathology in Alzheimer's disease. Stem Cell Rep. 9, 1885–1897. https://doi.org/10.1016/j.stemcr.2017.10.016.

Patel, A.B., Shaikh, S., Jain, K.R., Desai, C., Madamwar, D., 2020. Polycyclic aromatic hydrocarbons: sources, toxicity, and remediation approaches. Front. Microbiol. https://doi.org/10.3389/fmicb.2020.562813.

Pierdominici, M., Maselli, A., Cecchetti, S., Tinari, A., Mastrofrancesco, A., Alfè, M., Gargiulo, V., Beatrice, C., Di Blasio, G., Carpinelli, G., Ortona, E., Giovannetti, A., Fiorito, S., 2014. Diesel exhaust particle exposure in vitro impacts T lymphocyte phenotype and function. Part. Fibre Toxicol. 11. https://doi.org/10.1186/s12989-014-0074-0.

Pirjola, L., Kuuluvainen, H., Timonen, H., Saarikoski, S., Teinilä, K., Salo, L., Datta, A., Simonen, P., Karjalainen, P., Kulmala, K., Rönkkö, T., 2019. Potential of renewable fuel to reduce diesel exhaust particle emissions. Appl. Energy 254. https://doi.org/10.1016/j.apenergy.2019.113636.

Qi, Y., Wei, S., Xin, T., Huang, C., Pu, Y., Ma, J., Zhang, C., Liu, Y., Lynch, I., Liu, S., Murphy, C., 2022. Passage of exogeneous fine particles from the lung into the brain in humans and animals. DOi: 10.1073/pnas.

Razak, N.H., Hashim, H., Yunus, N.A., Klemeš, J.J., 2021. Reducing diesel exhaust emissions by optimisation of alcohol oxygenates blend with diesel/biodiesel. J. Clean. Prod. 316. https://doi.org/10.1016/j.jclepro.2021.128090.

Riederer, E., Cang, C., Ren, D., 2022. Annual review of pharmacology and toxicology lysosomal ion channels: what are they good for and are they druggable targets? Annu. Rev. Pharmacol. Toxicol. 2023 (63), 19–41. https://doi.org/10.1146/annurev-pharmtox-051921.

Saarikoski, S., Järvinen, A., Markkula, L., Aurela, M., Kuittinen, N., Hoivala, J., Barreira, L.M.F., Aakko-Saksa, P., Lepistö, T., Marjanen, P., Timonen, H., Hakkarainen, H., Jalava, P., Rönkkö, T., 2024. Towards zero pollution vehicles by advanced fuels and exhaust aftertreatment technologies. Environ. Pollut. 347. https://doi.org/10.1016/j.envpol.2024.123665.

Sabogal-Guáqueta, A.M., Marmolejo-Garza, A., Trombetta-Lima, M., Oun, A., Hunneman, J., Chen, T., Koistinaho, J., Lehtonen, S., Kortholt, A., Wolters, J.C., Bakker, B.M., Eggen, B.J.L., Boddeke, E., Dolga, A., 2023. Species-specific metabolic reprogramming in human and mouse microglia during inflammatory pathway induction. Nat. Commun. 14. https://doi.org/10.1038/s41467-023-42096-7.

Sardiello, M., Palmieri, M., Ronza, A.D., Medina, D.L., Valenza, M., Gennarino, V.A., Di Malta, C., Donaudy, F., Embrione, V., Polishchuk, R.S., Banfi, S., Parenti, G., Cattaneo, E., Ballabio, A., 2009. A gene network regulating lysosomal biogenesis and function. Science 1979 (325), 473–477. https://doi.org/10.1126/science.1174447.

Schmid, B., Prehn, K.R., Nimsanor, N., Garcia, B.I.A., Poulsen, U., Jørring, I., Rasmussen, M.A., Clausen, C., Mau-Holzmann, U.A., Ramakrishna, S., Muddashetty, R., Steeg, R., Bruce, K., Mackintosh, P., Ebneth, A., Holst, B., Cabrera-Socorro, A., 2020. Corrigendum to "Generation of a set of isogenic, gene-edited iPSC lines homozygous for all main APOE variants and an APOE knock-out line.". Stem Cell Res. 48. https://doi.org/10.1016/j.scr.2020.102005.

Schmid, B., Prehn, K.R., Nimsanor, N., Garcia, B.I.A., Poulsen, U., Jørring, I., Rasmussen, M.A., Clausen, C., Mau-Holzmann, U.A., Ramakrishna, S., Muddashetty, R., Steeg, R., Bruce, K., Mackintosh, P., Ebneth, A., Holst, B., Cabrera-Socorro, A., 2019. Generation of a set of isogenic, gene-edited iPSC lines homozygous for all main APOE variants and an APOE knock-out line. Stem Cell Res. 34. https://doi.org/10.1016/j.scr.2018.11.010.

Seo, S., Jang, M., Kim, H., Sung, J.H., Choi, N., Lee, K., Kim, H.N., 2023. Neuro-glia-vascular-on-a-chip system to assess aggravated neurodegeneration via brain endothelial cells upon exposure to diesel exhaust particles. Adv. Funct. Mater. 33. https://doi.org/10.1002/adfm.202210123.

Shkirkova, K., Lamorie-Foote, K., Zhang, N., Li, A., Diaz, A., Liu, Q., Thorwald, M.A., Godoy-Lugo, J.A., Ge, B., D'agostino, C., Zhang, Z., Mack, W.J., Sioutas, C., Finch, C. E., Mack, W.J., Zhang, H., 2022. Neurotoxicity of Diesel Exhaust Particles. J. Alzheimer's Dis. 89, 1263–1278. https://doi.org/10.3233/JAD-220493.

Speicher, A.M., Wiendl, H., Meuth, S.G., Pawlowski, M., 2019. Generating microglia from human pluripotent stem cells: novel in vitro models for the study of neurodegeneration. Mol. Neurodegener. https://doi.org/10.1186/s13024-019-0347-z.

Udayar, V., Chen, Y., Sidransky, E., Jagasia, R., 2022. Lysosomal dysfunction in neurodegeneration: emerging concepts and methods. Trends Neurosci. 45, 184–199. https://doi.org/10.1016/j.tins.2021.12.004.

Ural, B.B., Caron, D.P., Dogra, P., Wells, S.B., Szabo, P.A., Granot, T., Senda, T., Poon, M. M.L., Lam, N., Thapa, P., Lee, Y.S., Kubota, M., Matsumoto, R., Farber, D.L., 2022. Inhaled particulate accumulation with age impairs immune function and

architecture in human lung lymph nodes. Nat. Med. 28, 2622–2632. https://doi.org/10.1038/s41591-022-02073-x.

Vanbrabant, K., Van Dam, D., Bongaerts, E., Vermeiren, Y., Bové, H., Hellings, N., Ameloot, M., Plusquin, M., De Deyn, P.P., Nawrot, T.S., 2024. Accumulation of ambient black carbon particles within key memory-related brain regions. JAMA Netw. Open, E245678. https://doi.org/10.1001/jamanetworkopen.2024.5678.

Villani, A., Benjaminsen, J., Moritz, C., Henke, K., Hartmann, J., Norlin, N., Richter, K., Schieber, N.L., Franke, T., Schwab, Y., Peri, F., 2019. Clearance by microglia depends on packaging of phagosomes into a unique cellular compartment. Dev. Cell 49, 77–88.e7. https://doi.org/10.1016/j.devcel.2019.02.014.

Vogel, C.F.A., Van Winkle, L.S., Esser, C., Haarmann-Stemmann, T., 2020. The aryl hydrocarbon receptor as a target of environmental stressors – Implications for pollution mediated stress and inflammatory responses. Redox Biol. https://doi.org/10.1016/j.redox.2020.101530.

Wang, X., Wang, Y., Bai, Y., Wang, P., Zhao, Y., 2019. An overview of physical and chemical features of diesel exhaust particles. J. Energy Inst. 92. https://doi.org/10.1016/j.joei.2018.11.006.

Wichmann, H.E., 2007. Diesel exhaust particles. Inhal. Toxicol. 19, 241–244. https://doi.org/10.1080/08958370701498075.

World Health Organization, 2021. WHO global air quality guidelines Particulate matter (PM2.5 and PM10), ozone, nitrogen dioxide, sulfur dioxide and carbon monoxide [WWW Document]. URL https://iris.who.int/handle/10665/345329 (accessed 12.13.23).

World Medical Association, 2013. World Medical Association declaration of Helsinki: Ethical principles for medical research involving human subjects. JAMA 310, 2191–2194. DOi: 10.1001/jama.2013.281053.

Wu, L., Lin, Y., Song, J., Li, L., Rao, X., Wan, W., Wei, G., Hua, F., Ying, J., 2023. TMEM175: a lysosomal ion channel associated with neurological diseases. Neurobiol. Dis. 185. https://doi.org/10.1016/j.nbd.2023.106244.

Yvanka de Soysa, T., Therrien, M., Walker, A.C., Stevens, B., 2022. Redefining microglia states: Lessons and limits of human and mouse models to study microglia states in neurodegenerative diseases. Semin. Immunol. 60. https://doi.org/10.1016/j.smim.2022.101651.

Zhang, W., Xiao, D., Mao, Q., Xia, H., 2023. Role of neuroinflammation in neurodegeneration development. Signal Transduct. Target. Ther. 8. https://doi.org/10.1038/s41392-023-01486-5.